JOURNAL OF PETROLOGY | VOLUME 47 | NUMBER 5 | PAGES 901–927 | 2006 | doi:10.1093/petrology/egi100

Mg–Al Sapphirine- and Ca–Al Hibonite-bearing Granulite Xenoliths from the Chyulu Hills Volcanic Field, Kenya

A. ULIANOV* AND A. KALT

UNIVERSITY OF NEUCHÂTEL, INSTITUTE OF GEOLOGY, RUE EMILE-ARGAND 11, CH-2007 NEUCHÂTEL, SWITZERLAND

RECEIVED APRIL 1, 2004; ACCEPTED DECEMBER 19, 2005
ADVANCE ACCESS PUBLICATION FEBRUARY 7, 2006

Basanites of the Chyulu Hills (Kenya Rift) contain mafic Mg–Al and Ca–Al granulite xenoliths. Their protoliths are interpreted as troctolitic cumulates; however, the original mineral assemblages were almost completely transformed by subsolidus reactions. Mg–Al granulites contain the minerals spinel, sapphirine, sillimanite, plagioclase, corundum, clinopyroxene, orthopyroxene and garnet, whereas Ca–Al granulites are characterized by hibonite, spinel, sapphirine, mullite, sillimanite, plagioclase, quartz, clinopyroxene, corundum, and garnet. In the Mg–Al granulites, the first generation of orthopyroxene and some spinel may be of igneous origin. In the Ca–Al granulites, hibonite (and possibly some spinel) are the earliest, possibly igneous, minerals in the crystallization sequence. Most pyroxene, spinel and corundum in Mg–Al and Ca–Al granulites formed by subsolidus reactions. The qualitative P–T *path derived from metamorphic reactions corresponds to subsolidus cooling, probably accompanied, or followed by, compression. Final equilibration was achieved at* $T \approx 600–740^\circ C$ *and* $P < 8$ *kbar, in the stability field of sillimanite. The early coexistence of corundum and pyroxenes (± spinel), as well as the association of sillimanite and sapphirine with clinopyroxene and the presence of hibonite, makes both types of granulite rare. The Ca–Al hibonite-bearing granulites are unique. Both types enlarge the spectrum of known Ca–Al–Mg-rich granulites worldwide.*

KEY WORDS: *granulite xenoliths; corundum; sapphirine; hibonite; Kenya Rift*

INTRODUCTION

The study of granulites provides important constraints on the nature of high-temperature to ultrahigh-temperature metamorphism in the Earth's crust. On the one hand, the chemical and isotopic compositions of granulites are useful tools for deciphering their origin and geodynamic setting (e.g. Jan & Howie, 1981; Downes, 1993; Kempton *et al.*, 2001). On the other hand, reaction textures and the *P–T* paths of granulites serve to unravel metamorphic processes and their causes (e.g. Bohlen, 1987, 1991; Harley, 1989; Kriegsman & Schumacher, 1999; Rickers *et al.*, 2001). The study of granulites from metamorphic terranes often benefits from the incorporation of both approaches (e.g. Möller *et al.*, 1998; Osanai *et al.*, 1998; Bhattacharya & Kar, 2002). Granulites are also a major tool for investigating the composition of the Earth's lower crust. Granulite xenoliths from volcanic rocks are traditionally considered in this context (e.g. Rudnick *et al.*, 1986; Rudnick, 1992; Downes, 1993; Huang *et al.*, 1995; Kempton *et al.*, 2001), with far less attention being paid to their metamorphic reaction paths (Christy, 1989; Dawson *et al.*, 1997). The overwhelming dominance of the geochemical approach to the study of granulitic xenoliths is partly justified, as a given section of the Earth's middle to lower crust, sampled by an ascending magma, may include rocks of different provenance, age and metamorphic evolution, juxtaposed by various tectonic processes (e.g. Downes *et al.*, 1990; Kempton *et al.*, 1990).

The studied granulite xenoliths from the Chyulu Hills, East African Rift, can yield information on both issues, the chemical composition of the Earth's lower crust, in this case that beneath the East African Rift, and the nature and conditions of metamorphic processes that affected it. Recent major and trace element studies on minerals and whole-rock samples have shown that the Mg–Al granulites, Ca–Al granulites and garnet–spinel

*Corresponding author. Present address: University of Lausanne, Institute of Mineralogy and Petrography, BFSH 2, CH-1015 Lausanne, Switzerland. Telephone: +0041 21 6924452. Fax: +0041 21 6924305. E-mail: Alexey.Ulianov@unil.ch

websterite xenoliths of the Chyulu Hills represent a series of gabbroic to troctolitic cumulates that seems to be related to arc magmatism (Ulianov *et al.*, in preparation; see the section on 'General chemical and petrographic features'). Combined with similarities to certain granulite terranes in Tanzania (see Discussion) this geochemical signature suggests that the xenoliths, and hence the crust and upper mantle beneath the Chyulu Hills, are of Pan-African age.

The igneous minerals in the protoliths of the Mg–Al and Ca–Al granulite xenoliths have, to a large degree, been replaced by subsolidus assemblages that provide important information on the P–T path and on phase relations in mafic Ca–Mg–Al-rich bulk compositions. Meta-igneous granulitic rocks rich in Mg, Al and Ca are rare. They tend to crystallize sapphirine and clinopyroxene, and apparently represent a special paragenetic family of granulites that was recognized by Christy (1989). This includes xenoliths from Stockdale (Meyer & Brookins, 1976), Delegate (Griffin & O'Reilly, 1986) and the Kerguelen Archipelago (Grégoire *et al.*, 1998), and granulites from the metamorphic terranes of Finero (Lensch, 1971; Sills *et al.*, 1983), Roan (Johansson & Möller, 1986), Dunkelsteinerwald (Carswell *et al.*, 1989), the Central Gneiss Belt of the Grenville Province (Grant, 1989), Ullared–Gällared (Möller, 1999) and several other, less well-characterized terranes.

The purpose of this paper is (1) to contribute to the general understanding of mineral assemblages and reactions in Ca–Mg–Al-rich mafic igneous protoliths under granulite-facies conditions and (2) to decipher the reaction paths of the studied granulites and discuss their possible geological significance. For this purpose, mineral assemblages, mineral compositions and reaction sequences are carefully described, P–T conditions are quantified when possible, and a qualitative P–T path is inferred.

GEOLOGICAL SETTING

The Chyulu Hills volcanic field is situated on the eastern flank of the Kenya rift some 150–200 km east of the rift axis, about 50 km NE of Mt. Kilimanjaro (Fig. 1). It consists of several hundred volcanic cones and lava flows forming a NW–SE-aligned chain ~100 km long. For the last decade, the Chyulu Hills have been subject to a number of detailed petrological (focused on xenoliths and alkaline volcanic rocks) and geophysical (gravity and seismological) studies (e.g. Henjes-Kunst & Altherr, 1992; Novak *et al.*, 1997; Ritter & Kaspar, 1997; Späth *et al.*, 2001). The seismic Moho has been detected at a depth of 44 km (the divide is not sharp) with a thickness of 20 km for the lower crust (Ritter & Kaspar, 1997). The lithosphere–asthenosphere boundary lies at ~107–120 km depth as suggested by the geobarometric estimates for high-P porphyroclastic garnet lherzolite xenoliths from the Chyulu volcanic rocks (Henjes-Kunst & Altherr, 1992; Altherr *et al.*, in preparation).

Volcanic activity within the Chyulu Hills is very young. The compositional spectrum of rocks ranges from foidites through less silica-undersaturated basanites to fractionated alkali basalts (Haug & Strecker, 1995; Späth *et al.*, 2001). Foidites are the oldest (1·4 Ma), whereas some of the alkali basalts were erupted in historical times (Haug & Strecker, 1995). Despite its young volcanicity, there are no indications for a recent asthenospheric upwelling or upwarping of the Moho beneath the Chyulu Hills volcanic field (Novak *et al.*, 1997; Ritter & Kaspar, 1997). The xenoliths used for this study were sampled from basanites of the Kwa Nthuku volcano in the northwestern part of the Chyulu Hills.

The Chyulu Hills are located within the Pan-African Mozambique mobile belt (Holmes, 1951) extending from the Arabian–Nubian Shield in the north via Ethiopia, Uganda, Kenya and Tanzania to Mozambique, Malawi and Madagascar in the south. The Mozambique belt includes several metamorphic domains with different ages and P–T histories (e.g. Shackleton, 1973; Key *et al.*, 1989; Stern & Dawoud, 1991; Pinna *et al.*, 1993; Appel *et al.*, 1998; Möller *et al.*, 1998, and references therein). It resulted from a complex series of subduction, collision and accretion events between approximately 750 and 615 Ma (e.g. Coolen *et al.*, 1982; Kröner *et al.*, 1987; Stern & Dawoud, 1991; Muhongo & Lenoir, 1994; Möller *et al.*, 1998, 2000; Muhongo *et al.*, 2001; Kröner *et al.*, 2003; Meert, 2003), related to the closure of the Mozambique ocean. The younger events within this time span are commonly termed 'Pan-African' (e.g. Möller *et al.*, 2000), whereas the older ones are often related to an 'East African orogen' (e.g. Stern, 1994; Meert, 2003). The older history of the Mozambique belt seems to vary with geographical position. Magmatic and metamorphic events have been dated at 800–820 Ma (e.g. Key *et al.*, 1989; Kebede *et al.*, 2001), at approximately 1000–1250 Ma (e.g. Pinna *et al.*, 1993; Kröner *et al.*, 1987; Evans *et al.*, 1999), at around 2000 Ma (e.g. Möller *et al.*, 1995, 1998) and in the Archaean (Bell & Dodson, 1981; Cahen *et al.*, 1984; Muhongo *et al.*, 2001).

Lithologically, the Mozambique belt is dominated by amphibolite-facies and lower grade metamorphic rocks and granitoids, but it also contains numerous granulite complexes. Together with the igneous complexes, the latter were the focus of most of the geochronological studies cited above and the subject of extensive petrological and geochemical investigations (e.g. Maaskant *et al.*, 1980; Sandiford *et al.*, 1987; Gichile, 1992; Pinna *et al.*, 1993; Möller *et al.*, 1995, 2000; Appel *et al.*, 1998). Therefore, the outcropping granulites play a major role in reconstructing Proterozoic metamorphic and

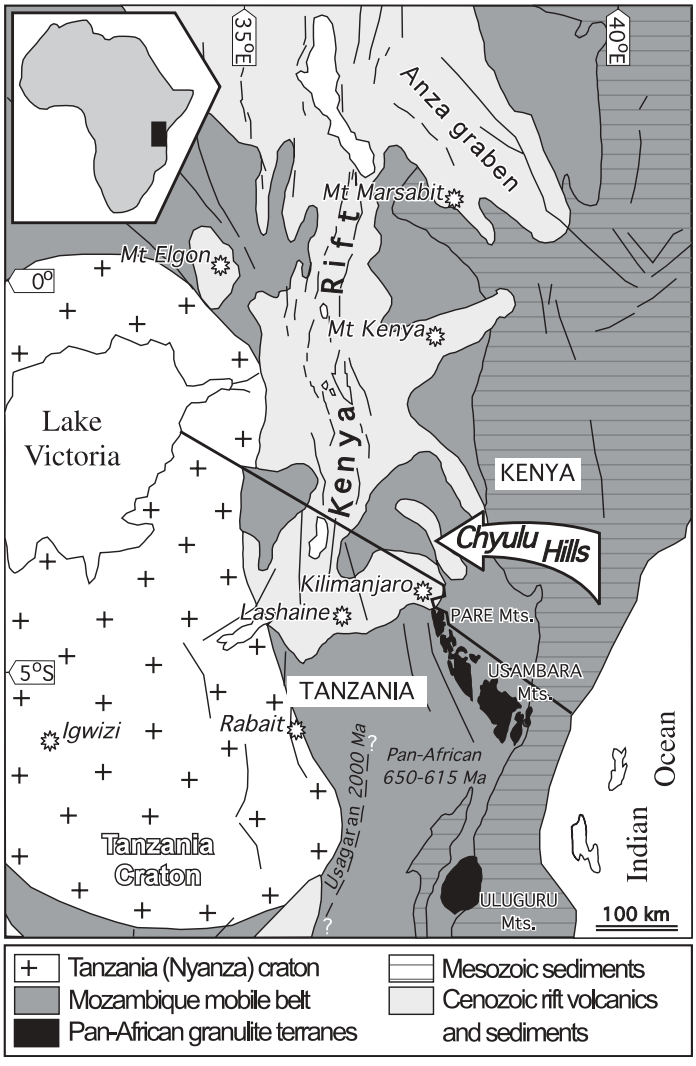

Fig. 1. Generalized geological map of Kenya, northern Tanzania, and parts of Uganda and Ethiopia, showing the principal tectonic units and the location of the Chyulu Hills volcanic field. The outcropping granulite terranes of NW Tanzania are after Möller *et al.* (2000) and the distribution of Cenozoic volcanic and sedimentary rocks in the region is after Williams (1970) and Baker *et al.* (1971).

geodynamic processes in the Mozambique belt. In contrast, few data are available for granulite xenoliths in volcanic edifices situated within the Mozambique belt of East Africa. They have been described from the Neogene volcanic rocks of the Lashaine volcano in northern Tanzania (Dawson, 1977; Jones *et al.*, 1983). As is the case with the granulite xenoliths of this study, those of Lashaine represent relics of an igneous suite metamorphosed into granulites (Jones *et al.*, 1983), but with a different chemical and mineralogical composition compared with the Chyulu xenoliths.

The local basement of the Chyulu Hills consists of hornblende and hornblende–biotite gneisses, migmatized and granitoid gneisses and subordinate garnet amphibolites and marbles (Saggerson, 1963; Omenge & Okelo, 1992). Granulites are rare. They form thin bands in gneisses, few of which are traceable for great distances (Saggerson, 1963). The granulites are calc-silicate in composition and contain andesine plagioclase, pyroxene (especially clinopyroxene), scapolite, garnet, epidote and in some cases quartz. They are lithologically different from the granulite xenoliths sampled by the young basanitic magmas. Because of the lack of isotopic and age data, both the outcropping basement granulites and the granulite xenoliths of the Chyulu Hills volcanic field cannot be *a priori* assigned to any of the above-described granulite occurrences in East Africa.

ANALYTICAL TECHNIQUES

Mineral analyses were made on a CAMECA SX50 microprobe equipped with four wavelength-dispersive

spectrometers at the Mineralogisch–Petrographisches Institut, University of Bern, and a CAMECA SX51 microprobe with five wavelength-dispersive spectrometers at the Mineralogisches Institut, University of Heidelberg. No systematic deviations were found in the control analyses performed on both machines. The microprobes were operated at a 15 kV accelerating voltage and a 20 nA beam current. The beam was focused to 1·5–2 μm for mafic phases, and to 5 or 10 μm for plagioclase. PAP correction was applied to the raw data. Natural and synthetic oxide and silicate standards were used for calibration. For spinel, corundum, sillimanite and plagioclase, Fe^{3+} and Fe^{2+} were calculated from stoichiometry. For other minerals, all Fe was taken as FeO.

Whole-rock major element abundances were determined on glass pills [for preparation technique, see Ulianov *et al.* (2005)] using a CAMECA SX50 microprobe at the Mineralogisch–Petrographisches Institut, University of Bern. The beam was rastered over an area of ~15 μm × 20 μm; operating conditions were the same as for minerals. Another set of analyses was obtained by X-ray fluorescence (XRF) on fused discs using a Philips PW2400 instrument at the Institut de Minéralogie et de Pétrographie, University of Fribourg. The results from both techniques appear consistent. In the following, we use the electron microprobe measurements because of their slightly better totals. Cr, Ni, Sr and Ba were also determined by XRF at the University of Fribourg.

GENERAL CHEMICAL AND PETROGRAPHIC FEATURES

The major element compositions and CIPW norms of the studied granulite xenoliths are presented in Table 1. The rocks are slightly silica-undersaturated, rich in Al and relatively enriched in Ca. The overall high Mg-number and very low abundances of high field strength elements (HFSE) and light rare earth elements (LREE) (Ulianov *et al.*, in preparation) suggest that the rocks represent a sequence of cumulates rather than crystallized melts. The CIPW normative compositions are dominated by plagioclase and olivine, with the normative 'troctolitic' component (plagioclase + olivine) ranging from 89·6 to 98·7%. The high Ni and very low Ti abundances in the rocks accord well with a troctolitic mineralogy of the protoliths. The cumulate sequence also includes websteritic lithologies finally equilibrated under mantle pressures and temperatures. They belong to the same major and trace element fractionation trend as the granulites, but are more magnesian and depleted in Si, Al, Ca and alkalis (Ulianov *et al.*, in preparation; see Discussion).

The mineral assemblage of the two studied Mg–Al sapphirine-bearing granulites (1904-3 and 1904-7) is spinel, sapphirine, sillimanite, plagioclase, ortho- and clinopyroxene, corundum, and garnet (Fig. 2a and b).

Table 1: Major and trace element compositions (in wt %) of the studied xenoliths and their CIPW norms

	1904-3	1904-7	1906-2	1904-9	1904-1
wt %					
SiO_2	46·51	47·65	46·39	50·18	49·66
TiO_2	0·01	0·01	0·01	0·05	0·01
Al_2O_3	18·09	23·20	20·34	23·58	24·59
FeO_t	9·27	5·39	9·39	4·57	4·76
MnO	0·11	0·08	0·11	0·06	0·06
MgO	16·01	9·61	12·25	6·34	6·06
CaO	8·12	10·32	8·59	10·68	10·11
Na_2O	1·74	2·82	2·37	3·55	3·72
K_2O	0·10	0·19	0·10	0·25	0·20
P_2O_5	0·02	0·06	0·01	0·05	0·03
LOI	0·11	0·41	0·12	0·43	0·28
Total	100·09	99·74	99·68	99·74	99·48
Mg-no.	75·5	76·1	69·9	71·2	69·4
ppm					
Cr	87	65	919	238	102
Ni	445	367	374	209	271
Sr	357	872	332	733	657
Ba	102	627	60	1155	955
Quartz	no	no	no	no	no
Orthoclase	0·59	1·13	0·59	1·49	1·19
Albite	14·71	22·22	20·12	29·63	29·90
Anorthite	40·20	50·36	42·77	47·94	50·15
Corundum	0·37	no	0·71	no	no
Nepheline	no	0·96	no	0·31	0·97
Diopside (Wo)	no	0·36	no	2·15	0·11
Diopside (En)	no	0·24	no	1·32	0·07
Diopside (Fs)	no	0·10	no	0·70	0·04
Hypersthene (En)	6·95	no	1·69	no	no
Hypersthene (Fs)	2·98	no	0·96	no	no
Olivine (Fo)	23·16	16·77	20·35	10·25	10·64
Olivine (Fa)	10·98	7·71	12·77	6·00	6·84
Ilmenite	0·02	0·02	0·02	0·10	0·02
Apatite	0·04	0·13	0·02	0·11	0·07

Mg-number = 100 × Mg/(Mg + Fe), all Fe as Fe^{2+}. LOI, loss on ignition.

The three studied Ca–Al hibonite-bearing granulites (1904-1, 1904-9, 1906-2) always show the assemblage spinel, sillimanite, clinopyroxene, quartz, plagioclase, corundum and garnet (Fig. 2c), but may additionally contain hibonite [$Ca(Al,Cr,Ti,Si,Mg,Fe^{2+})_{12}O_{19}$, 1904-1, 1904-9], mullite (1904-9) and sapphirine (1904-1). Both rock types display a wealth of reaction textures.

Two out of five granulite xenoliths analysed in this study are banded, composed of layers of more mafic

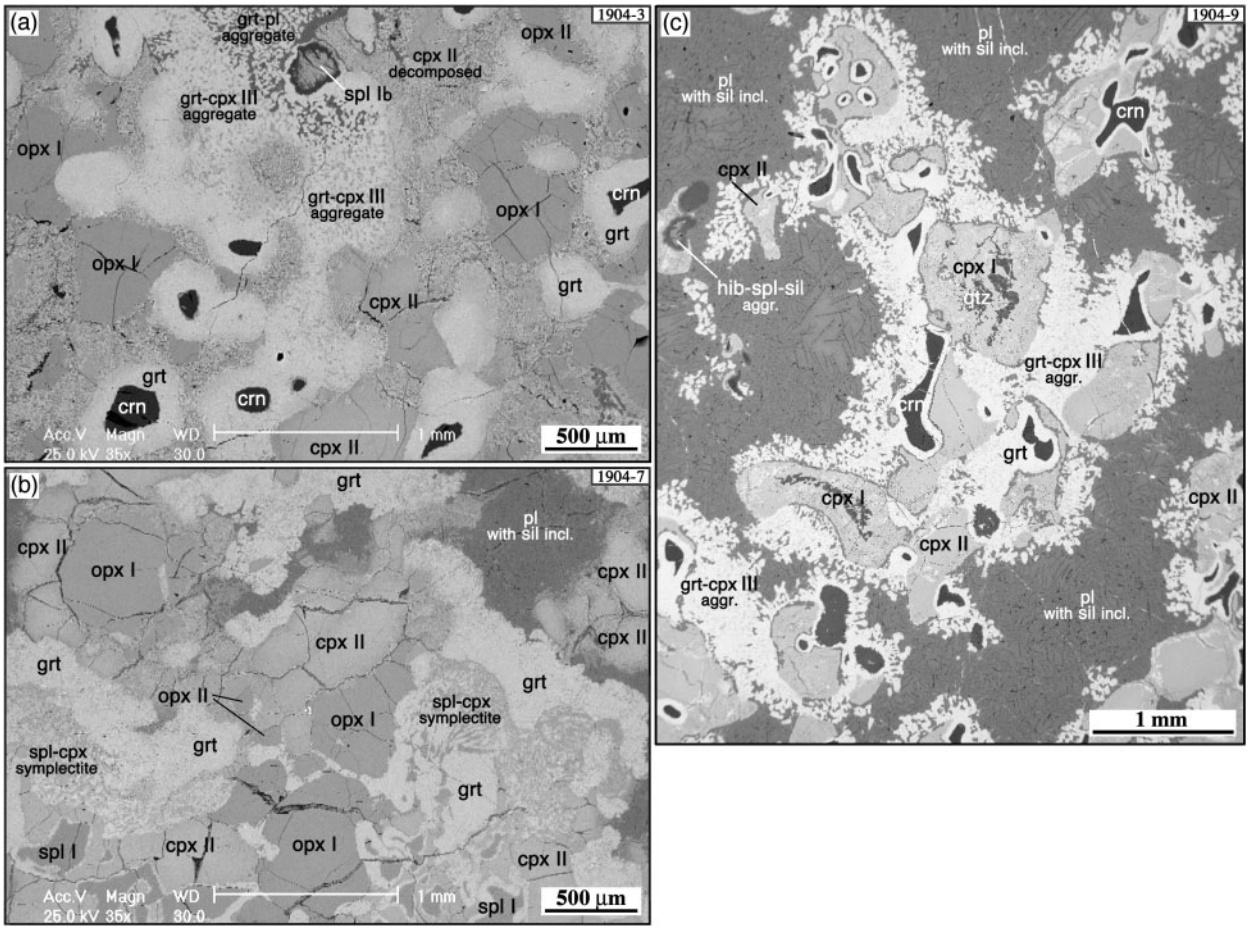

Fig. 2. Back-scattered electron images showing the textures and mineralogy of the studied xenoliths: (a) and (b) Mg–Al two-pyroxene sapphirine-bearing granulites (1904-3; 1904-7); (c) Ca–Al clinopyroxene hibonite-bearing granulite (1904-9). Mineral abbreviations after Kretz (1983).

and more felsic granulite. Mafic and felsic layers contain the same minerals but their modes differ. We interpret this banding to be of magmatic origin, as there are no indications of metamorphic differentiation processes or deformation (e.g. foliation) that could, in principle, also produce banding. Fabrics within the layers are isotropic and all of the reaction textures described in the section on textures and mineral compositions have developed in the absence of anisotropic stress.

The studied xenoliths are greatly affected by late-stage alteration. As a rule, garnet is replaced by kelyphite. The kelyphite is always extremely fine-grained. It consists of very Al-rich orthopyroxene, plagioclase and spinel. Clinopyroxene suffered incongruent melting and is often decomposed into a mixture of secondary diopside, plagioclase and quenched melt. Similar phenomena have been described elsewhere; for example, in some lherzolite xenoliths from Hawaii (White, 1966), in garnet lherzolites from South African kimberlites (Carswell, 1975) and in a sapphirine-bearing granulite xenolith from the Delegate pipe in New South Wales, Australia (Griffin & O'Reilly, 1986). These overprints are probably caused by fast heating and decompression in the host basanitic magma. Henceforth, we refer to the primary mineral compositions only (see Tables 2 and 3).

TEXTURES AND MINERAL COMPOSITIONS

Mg–Al sapphirine-bearing granulites

The two studied Mg–Al sapphirine-bearing granulites (specimens 1904-3 and 1904-7) are petrographically similar to each other, although there are some distinctions. Xenolith 1904-3 is rather fine-grained, more mafic and appears mineralogically homogeneous. Xenolith 1904-7 is clearly banded, with more mafic (pyroxene-Rich) and more felsic (plagioclase-Rich) layers. Pyroxenes, plagioclase and garnet dominate, corundum and spinel are essential (5–15 vol. %), sapphirine is relatively rare. The

Table 2: Representative electron microprobe analyses of minerals from the Mg–Al sapphirine-bearing granulites

	1904-3																				
	OPX I	OPX II		CPX II			CPX III	SPL Ib associated with:				CRN		SPR	SIL	PL				GRT	
	cpx lam.				10 μm		aggr/	pyroxene		spr and sil				mantle	mantle		grt–pl	enve-	enve-	aggr/	relict
	integr.	core	rim	core	from rim	rim	grt	core	rim	core	rim	core	rim	on spl	on spl	core	aggr.	lope	lope	cpx	
SiO_2	55·27	56·21	55·92	53·85	53·68	53·39	54·99	0·02	0·05	0·02	0·02	0·02	0·02	11·17	36·82	62·74	63·14	63·91	63·64	41·20	40·99
TiO_2	—	—	0·01	0·04	0·02	—	—	0·01	0·01	0·01	—	—	0·02	0·02	—					0·01	—
V_2O_3										—	—										
Al_2O_3	2·69	2·03	2·17	8·02	11·56	11·25	8·83	65·95	65·85	66·92	67·42	99·37	100·06	66·19	62·39	23·71	23·33	22·93	23·13	23·14	22·67
Cr_2O_3	0·02	0·01	0·01	—	0·05	—	0·08	0·15	0·25	0·13	0·15	0·03	0·11	0·14	0·01					0·02	0·04
FeO_t	9·87	10·08	9·90	3·11	2·60	2·75	3·10	13·02	13·20	12·72	12·37	0·23	0·37	4·29	0·55	0·07	0·40	0·18	0·13	14·45	14·91
MnO	0·07	0·02	0·10	0·02	0·04	—	0·10	0·08	0·07	0·03	0·01	—	0·04	—	—					0·29	0·27
NiO	0·25	0·27	0·23	0·13	0·08	0·03	0·12	1·40	1·42	1·66	1·63			0·53	0·02					0·05	0·01
ZnO								0·85	0·60	0·69	0·68										
MgO	30·21	32·04	32·01	12·70	10·85	10·97	12·22	18·85	19·15	18·50	18·08	0·01	—	17·05	—					17·80	17·25
CaO	1·29	0·21	0·23	19·38	17·45	17·47	16·66	—	—	—	—	—	0·01	—	0·01	4·38	4·11	3·64	3·89	3·86	4·19
SrO																0·29	0·26	0·16	0·32		
BaO																0·07	0·05	—	—		
Na_2O	0·45	0·07	0·11	3·23	4·58	4·56	4·57			0·01	0·01	0·02	0·01	0·02	0·01	8·56	8·62	9·01	8·91	—	—
K_2O	0·02	—	—	0·01	0·00	—	—			—	—	—	—	—	—	0·99	1·09	1·02	0·96	—	—
Total	100·13	100·95	100·70	100·49	100·91	100·42	100·66	100·33	100·61	100·69	100·37	99·69	100·64	99·41	99·81	100·81	101·00	100·85	100·97	100·81	100·33
Si	1·943	1·952	1·947	1·929	1·900	1·901	1·953	0·001	0·001	0·000	0·001	0·000	0·000	1·322	0·997	2·768	2·781	2·810	2·799	2·972	2·981
Ti	0·000	0·000	0·000	0·001	0·001	0·000	0·000	0·000	0·000	0·000	0·000	0·000	0·000	0·002	0·000					0·000	0·000
Al	0·111	0·083	0·089	0·339	0·482	0·472	0·369	1·965	1·955	1·986	2·005	1·995	1·992	9·232	1·991	1·233	1·211	1·188	1·198	1·967	1·943
Cr	0·001	0·000	0·000	0·000	0·002	0·000	0·002	0·003	0·005	0·003	0·003	0·000	0·001	0·013	0·000					0·001	0·002
Fe^{3+}								0·031	0·037	0·010	0·000	0·003	0·005		0·012	0·003	0·015	0·006	0·005	0·000	
Fe^{2+}	0·290	0·293	0·288	0·093	0·077	0·082	0·092	0·244	0·241	0·257	0·261	0·000	0·000	0·425	0·000	0·000	0·000	0·000	0·000	0·872	0·907
Mn	0·002	0·001	0·003	0·001	0·001	0·000	0·003	0·002	0·001	0·001	0·000	0·000	0·001	0·000	0·000					0·017	0·017
Ni	0·007	0·007	0·006	0·004	0·002	0·001	0·003	0·028	0·029	0·034	0·033			0·051	0·000					0·003	0·001
Zn								0·016	0·011	0·013	0·013				0·000						
Mg	1·583	1·659	1·661	0·678	0·573	0·582	0·647	0·710	0·719	0·695	0·680	0·000	0·000	3·009	0·000					1·914	1·870
Ca	0·049	0·008	0·009	0·744	0·662	0·666	0·634	0·000	0·000	0·000	0·000	0·000	0·000	0·000	0·000	0·207	0·194	0·172	0·183	0·298	0·326
Sr																0·007	0·007	0·004	0·008		
Ba																0·001	0·001	0·000	0·000		
Na	0·031	0·005	0·007	0·225	0·314	0·315	0·315	0·000	0·000	0·001	0·001	0·001	0·000	0·004	0·001	0·733	0·736	0·768	0·760	0·000	0·000
K	0·001	0·000	0·000	0·000	0·000	0·000	0·000	0·000	0·000	0·000	0·000	0·000	0·000	0·000	0·000	0·056	0·061	0·057	0·054	0·000	0·000
Sum	4·017	4·008	4·012	4·013	4·014	4·019	4·018	3·000	3·000	3·000	2·997	2·000	1·999	14·058	3·002	5·008	5·006	5·005	5·007	8·044	8·047
Mg-no.	84·5	84·99	85·22	87·9	88·2	87·7	87·6	74·4	74·9	73·0	72·3									68·7	67·3
Al^{IV}	0·040	0·039	0·041	0·058	0·086	0·079	0·028														
Al^{VI}	0·071	0·044	0·048	0·281	0·396	0·394	0·341														

	1904-7																				
	OPX I	OPX II		OPX II		CPX II			CPX III	CPX IV		SPL Ia		SPL Ib		CRN		SPR	SIL	PL		GRT
	cpx lam.			recrystallized														mantle	mantle			
	integr.	core	rim	core	rim	core	rim	rim		core	rim	core	core	core	core	core	rim	on spl	on spl	core	rim	relict
SiO_2	54·12	56·59	56·47	56·55	56·36	53·09	54·52	50·84	55·68	46·03	49·08	—	—	0·02	—	—	0·04	12·28	36·96	59·20	59·7	41·54
TiO_2	—	—	0·01	—	0·02	0·05	0·04	0·03	0·03	0·01	—	0·01	—	0·02	0·01	—	0·02	—	0·01			—
V_2O_3																						
Al_2O_3	3·04	1·17	1·63	1·27	1·97	6·81	9·39	14·49	8·53	22·78	19·55	66·05	66·82	66·58	66·25	99·41	98·84	65·32	61·67	26·04	25·79	23·16
Cr_2O_3	—	0·03	0·02	—	—	0·03	—	0·01	—	—	0·03	0·63	0·33	0·28	0·30	0·11	0·10	0·06	0·02			—
FeO_t	9·19	9·84	9·78	9·58	9·81	3·15	2·10	1·80	2·53			12·37	12·68	12·21	13·06	0·10	0·30	3·31	0·29	—	0·01	13·70
MnO	0·10	0·04	0·02	0·08	0·06	0·10	0·05	0·00	0·02	1·64	1·40	0·06	0·02	0·01	0·04	0·05	—	—	—			0·27
NiO	0·21	0·21	0·17	0·13	0·15	0·04	0·07	0·14	0·05	—	0·03	1·23	0·90	1·32	1·50			—	—			0·05
ZnO										0·03	0·05	0·36	0·23	0·30	0·37			0·39	0·03			
MgO	30·53	32·73	32·6	32·6	32·89	14·37	12·36	9·96	12·56	6·95	7·91	19·42	19·78	19·26	19·25	—	0·01	18·16	0·14			17·83
CaO	1·49	0·26	0·22	0·30	0·20	21·27	18·21	18·81	16·41	18·83	17·87	—	—	0·01	—	0·01	0·01	—	0·06	7·49	7·34	4·32
SrO																				0·15	0·13	
BaO																				0·05	0·08	
Na_2O	0·48	0·03	0·04	0·05	0·04	1·73	3·94	3·89	4·73	3·75	4·42							0·03	0·02	7·20	7·33	—
K_2O	—	—	—		0·01	0·01	—	0·02	—	0·01	0·02							—	0·01	0·40	0·39	—
Total	99·17	100·91	100·96	100·57	100·93	100·66	100·69	100·00	100·53	100·03	100·36	100·14	100·77	100·00	100·79	99·68	99·32	99·55	99·20	100·53	100·77	100·89
Si	1·920	1·965	1·958	1·967	1·946	1·908	1·932	1·818	1·97	1·645	1·740	0·000	0·000	0·000	0·000	0·000	0·001	1·443	1·006	2·634	2·648	2·986
Ti	0·000	0·000	0·000	0·000	0·000	0·001	0·001	0·001	0·001	0·000	0·000	0·000	0·000	0·000	0·000	0·000	0·000	0·000	0·000			0·000
Al	0·127	0·048	0·067	0·052	0·080	0·288	0·392	0·611	0·356	0·959	0·817	1·963	1·969	1·979	1·961	1·996	1·993	9·041	1·979	1·366	1·348	1·962
Cr	0·000	0·001	0·000	0·000	0·000	0·001	0·000	0·000	0·000	0·000	0·001	0·013	0·007	0·006	0·006	0·001	0·001	0·006	0·000			0·000
Fe^{3+}										0·000	0·000	0·024	0·025	0·014	0·033	0·001	0·004	0·000	0·007			0·000
Fe^{2+}	0·273	0·286	0·283	0·279	0·283	0·095	0·062	0·054	0·075	0·049	0·042	0·237	0·240	0·244	0·241	0·000	0·001	0·325	0·000	0·000	0·000	0·824
Mn	0·003	0·001	0·000	0·002	0·002	0·003	0·001	0·000	0·001	0·000	0·001	0·001	0·000	0·000	0·001	0·001	0·000	0·000	0·000			0·017
Ni	0·006	0·006	0·005	0·004	0·000	0·001	0·002	0·004	0·001	0·001	0·001	0·025	0·018	0·027	0·030			0·037	0·001			0·003
Zn												0·007	0·004	0·006	0·007							
Mg	1·615	1·694	1·685	1·690	1·693	0·770	0·653	0·531	0·663	0·370	0·418	0·730	0·737	0·724	0·721	0·000	0·000	3·179	0·006			1·910
Ca	0·057	0·010	0·008	0·011	0·007	0·819	0·691	0·721	0·622	0·721	0·679	0·000	0·000	0·000	0·000	0·000	0·000	0·000	0·002	0·357	0·349	0·333
Sr																				0·004	0·003	
Ba																				0·001	0·001	
Na	0·033	0·002	0·003	0·004	0·003	0·121	0·270	0·270	0·325	0·260	0·304					0·000	0·000	0·006	0·001	0·621	0·630	0·000
K	0·000	0·000	0·000	0·000	0·000	0·000	0·000	0·001	0·000	0·000	0·001					0·000	0·000	0·000	0·000	0·022	0·022	0·000
Sum	4·033	4·012	4·010	4·009	4·015	4·007	4·006	4·011	4·013	4·005	4·003	3·000	3·000	3·000	3·000	2·000	2·000	14·037	3·001	5·005	5·001	8·034
Mg-no.	85·5	85·6	85·6	85·8	85·7	89·0	91·3	90·8	89·8	88·3	90·9	75·5	75·4	74·8	74·9							69·9
Al^{IV}	0·047	0·024	0·032	0·024	0·039	0·085	0·062	0·171	0·017	0·350	0·256											
Al^{VI}	0·080	0·025	0·035	0·028	0·042	0·203	0·330	0·440	0·340	0·610	0·561											

Mg-number = $100 \times Mg/(Mg + Fe^{2+})$. —, not detected.

Table 3: Representative electron microprobe analyses of minerals from the Ca–Al hibonite-bearing granulites

	1906-2																					
	CPX I		CPX II			CPX III	SPL I		SPL I		SPL II		CRN				SIL		PL		GRT	
				20 μm		aggr/	grain 1		grain 2				individual		with spl II		rim/	rim/		enve-	aggr/	relict
	core	core	core	from rim	rim	grt	core	rim	core	rim	core	rim	core	rim	core	rim	Cr-spl I	spl I	core	lope	cpx	near spl
SiO_2	54·74	54·76	53·19	52·67	52·58	52·71	—	0·02	0·01	0·01	0·06	0·06	—	0·04	0·03	—	37·05	37·12	60·88	61·52	40·83	40·67
TiO_2	—	0·01	0·06	0·04	0·03	0·05	0·01	—	—	—	0·02	0·02	—	—	—	—	—	0·01			0·03	0·02
V_2O_3							0·04	—	0·04	—	0·09	0·10					—					
Al_2O_3	4·80	5·30	8·17	10·11	9·18	9·40	63·08	63·19	55·40	55·27	25·08	24·32	98·91	99·36	92·28	98·68	60·75	62·96	25·14	24·21	22·97	22·95
Cr_2O_3	0·05	—	0·10	0·28	0·45	—	3·27	3·13	11·18	10·82	39·69	39·44	0·23	0·71	6·95	0·28	1·96	0·06			—	0·05
FeO_t	3·57	3·60	3·90	3·25	3·29	3·42	13·94	14·10	15·38	15·18	24·71	25·14	0·35	0·55	0·90	0·53	0·64	0·37	0·03	0·29	14·29	14·65
MnO	0·03	—	0·02	—	0·06	0·04	0·04	—	—	—	0·15	0·01	—	—	—	—	—	0·02			0·26	0·15
NiO	0·16	0·13	0·12	0·13	0·17	0·18	2·13	2·08	1·63	1·59	0·39	0·47	0·01	—	0·02	0·03	—	0·03			0·02	—
ZnO							1·84	1·79	2·76	2·64	1·63	1·66					—				—	
MgO	13·92	13·65	11·74	11·29	11·72	11·98	16·41	16·44	14·14	14·20	8·54	8·37	0·02	—	0·02	0·01	0·01	0·01			14·95	14·35
CaO	20·50	20·13	18·65	19·24	19·55	19·37	0·01	—	—	—	0·01	—	—	0·02	—	—	—	0·03	6·37	5·59	7·64	7·94
SrO																			0·11	0·15		
BaO																			—	0·02		
Na_2O	2·42	2·71	3·64	3·5	3·27	3·4	0·06	0·05	0·09	0·08	0·04	0·05	—	—	0·02	—	—	—	8·11	8·30	0·03	0·01
K_2O	—	—	0·01	0·01	0·01	0·01	—	0·01	—	—	—	—	0·02	0·01	—	0·01	—	—	0·29	0·36		—
Total	100·19	100·29	99·59	100·51	100·31	100·56	100·83	100·82	100·62	99·78	100·40	99·65	99·54	100·69	100·21	99·54	100·82	100·60	100·92	100·44	101·03	100·79
Si	1·976	1·973	1·929	1·890	1·895	1·893	0·000	0·001	0·000	0·000	0·002	0·002	0·000	0·001	0·000	0·000	1·004	0·997	2·688	2·726	2·969	2·971
Ti	0·000	0·000	0·002	0·001	0·001	0·001	0·000	0·000	0·000	0·000	0·000	0·001	0·000	0·000	0·000	0·000	0·000	0·000			0·002	0·001
V							0·001	0·000	0·001	0·000	0·002	0·003										
Al	0·204	0·225	0·349	0·427	0·390	0·398	1·917	1·920	1·755	1·761	0·922	0·903	1·991	1·981	1·890	1·988	1·939	1·993	1·308	1·264	1·969	1·976
Cr	0·001	0·000	0·003	0·008	0·013	0·000	0·067	0·064	0·238	0·231	0·979	0·982	0·003	0·010	0·095	0·004	0·042	0·001			0·000	0·003
Fe^{3+}							0·018	0·018	0·011	0·011	0·096	0·110	0·005	0·008	0·013	0·008	0·012	0·008	0·001	0·011		
Fe^{2+}	0·108	0·108	0·118	0·098	0·099	0·103	0·283	0·286	0·334	0·332	0·549	0·552	0·000	0·000	0·000	0·000	0·003	0·000	0·000	0·000	0·869	0·895
Mn	0·001	0·000	0·001	0·000	0·002	0·001	0·001	0·000	0·000	0·000	0·004	0·000	0·000	0·000	0·000	0·000	0·000	0·000			0·016	0·009
Ni	0·005	0·004	0·003	0·004	0·005	0·005	0·044	0·043	0·035	0·035	0·010	0·012	0·000	0·000	0·000	0·000		0·001			0·001	0·000
Zn							0·035	0·034	0·055	0·053	0·038	0·039										
Mg	0·749	0·733	0·635	0·604	0·630	0·641	0·631	0·632	0·566	0·572	0·397	0·393	0·000	0·000	0·000	0·000	0·000	0·000			1·621	1·562
Ca	0·793	0·777	0·725	0·739	0·755	0·745	0·000	0·000	0·000	0·000	0·000	0·000	0·000	0·000	0·000	0·000	0·000	0·001	0·301	0·265	0·595	0·621
Sr																			0·003	0·004		
Ba																			0·000	0·000		
Na	0·170	0·189	0·256	0·243	0·229	0·237	0·003	0·002	0·005	0·004	0·002	0·003	0·000	0·000	0·001	0·000	0·000	0·000	0·694	0·713	0·004	0·001
K	0·000	0·000	0·001	0·001	0·000	0·000	0·000	0·000	0·000	0·000	0·000	0·000	0·000	0·000	0·000	0·000	0·000	0·000	0·016	0·020	0·000	0·000
Sum	4·007	4·009	4·021	4·014	4·019	4·025	3·000	3·000	3·000	3·000	3·000	3·000	2·000	2·000	2·000	2·000	3·000	3·002	5·012	5·004	8·046	8·039
Mg-no.	87·4	87·2	84·3	86·0	86·4	86·2	69·0	68·8	62·9	63·3	42·0	41·6									63·6	63·6
Al^{IV}	0·018	0·018	0·050	0·097	0·088	0·082																
Al^{VI}	0·187	0·207	0·300	0·331	0·302	0·317																

	1904-1																				
	CPX I		CPX II		CPX III	SPL I		SPL I		SPL II		CRN				SIL	SPR	HIBONITE		PL		GRT
			10 mm		aggr/	grain 1		grain 2				individual		with spl II		mantle				core	enve-	incl.
	core	core	from rim	rim	grt	core	rim	core	rim	core	rim	core	rim	core	rim	on spl I		core	rim		lope	in cpx
SiO_2	54·26	53·32	52·03	52·23	51·46	0·05	0·01	0·01	0·03	0·04	0·01	—	0·04	0·04	0·10	36·92	10·97	2·33	2·28	59·46	59·71	40·34
TiO_2	0·01	0·08	0·14	0·14	0·06	0·01	—	—	0·02	0·05	—	0·01	0·02	0·02	0·01	—	—	2·14	2·46			0·00
V_2O_3																						
Al_2O_3	5·10	7·52	11·33	10·50	9·93	64·89	65·21	63·15	63·01	28·00	27·99	99·43	98·95	99·31	92·64	62·59	66·53	82·27	81·97	26·12	26·11	22·50
Cr_2O_3	0·08	—	0·02	0·01	0·00	1·72	1·86	3·02	2·94	39·31	39·07	0·16	0·14	0·45	7·70	0·32	0·81	0·38	0·40			0·00
FeO_t	2·87	3·87	2·19	2·23	2·87	13·22	13·28	14·41	14·46	21·75	22·33	0·20	0·27	0·26	0·43	0·25	4·06	2·12	2·17	0·02	0·06	13·66
MnO	0·01	0·03	0·03	—	0·04	0·03	0·07	0·04	0·01	0·09	0·08	—	0·03	—	—	0·01	0·03	0·01	0·02			0·14
NiO	0·14	0·12	0·15	0·11	0·09	1·51	1·51	1·44	1·51	0·31	0·34						0·40					0·05
ZnO						1·40	1·25	1·68	1·73	1·35	1·29							0·16	0·26			
MgO	14·30	12·64	11·61	12·10	12·15	17·46	17·32	16·75	16·94	9·56	9·57	0·01	—	—	0·01	0·03	17·14	2·00	2·04			11·73
CaO	20·43	20·79	20·47	20·71	20·11	—	—	0·01	0·01	0·04	0·10	—	0·02	0·01	0·04	0·04	0·02	8·45	8·40	7·68	7·27	11·06
SrO																				0·03	0·15	
BaO																				0·01	0·06	
Na_2O	2·45	2·48	2·83	2·62	2·63							—	—	0·01	0·01	—	0·02	0·04	0·01	7·16	7·28	0·01
K_2O	0·01	0·01	—	0·02	0·01							0·01	—	—	—	—	—	—	—	0·43	0·46	0·00
Total	99·66	100·85	100·79	100·67	99·35	100·30	100·54	100·50	100·67	100·50	100·79	99·82	99·47	100·10	100·93	100·16	99·98	99·91	100·00	100·91	101·09	99·49
Si	1·964	1·916	1·855	1·866	1·868	0·001	0·000	0·000	0·001	0·001	0·000	0·000	0·001	0·001	0·002	0·996	1·292	0·264	0·258	2·634	2·641	2·999
Ti	0·000	0·002	0·004	0·004	0·002	0·000	0·000	0·000	0·000	0·001	0·000	0·000	0·000	0·000	0·000	0·000	0·000	0·183	0·209			0·000
V																						
Al	0·218	0·319	0·476	0·442	0·425	1·957	1·962	1·920	1·913	1·011	1·007	1·995	1·993	1·989	1·886	1·991	9·233	10·982	10·945	1·364	1·361	1·972
Cr	0·002	0·000	0·001	0·000	0·000	0·035	0·038	0·062	0·060	0·952	0·944	0·002	0·002	0·006	0·105	0·007	0·075	0·034	0·036			0·000
Fe^{3+}						0·006	0·000	0·018	0·025	0·033	0·049	0·003	0·004	0·003	0·006	0·006		0·000	0·000	0·001	0·002	
Fe^{2+}	0·087	0·116	0·065	0·067	0·087	0·277	0·284	0·293	0·286	0·524	0·522	0·000	0·000	0·000	0·000	0·000	0·399	0·201	0·206	0·000	0·000	0·849
Mn	0·000	0·001	0·001	0·003	0·001	0·001	0·002	0·001	0·000	0·002	0·002	0·000	0·000	0·000	0·000	0·000	0·002	0·001	0·001			0·009
Ni	0·004	0·003	0·004	0·000	0·003	0·031	0·031	0·030	0·031	0·008	0·008	0·000					0·038					0·003
Zn						0·026	0·024	0·032	0·033	0·031	0·029							0·013	0·022			
Mg	0·771	0·677	0·617	0·644	0·657	0·666	0·659	0·644	0·650	0·437	0·436	0·000	0·000	0·000	0·000	0·001	3·009	0·338	0·345			1·300
Ca	0·793	0·801	0·782	0·793	0·782	0·000	0·000	0·000	0·000	0·001	0·003	0·000	0·000	0·000	0·001	0·001	0·003	1·025	1·019	0·364	0·344	0·881
Sr																				0·001	0·004	
Ba																				0·000	0·001	
Na	0·172	0·173	0·195	0·181	0·185							0·000	0·000	0·000	0·000	0·000	0·004	0·009	0·002	0·615	0·624	0·002
K	0·001	0·000	0·000	0·001	0·000							0·000	0·000	0·000	0·000	0·000	0·000	0·000	0·000	0·025	0·026	0·000
Sum	4·012	4·008	4·000	4·001	4·011	3·000	3·000	3·000	3·000	3·000	3·000	2·000	2·000	2·000	2·000	3·002	14·056	13·050	13·044	5·003	5·003	8·015
Mg-no.	89·9	85·4	90·5	90·6	88·3	70·6	69·9	68·7	69·4	45·5	45·5											60·5
Al^{IV}	0·024	0·075	0·145	0·134	0·122																	
Al^{VI}	0·195	0·244	0·331	0·308	0·303																	

Table 3: Continued

	1904-9																				
	CPX I		CPX II		CPX III	SPL I		SPL I		CRN		SIL	MULLITE		HIBONITE				PL		GRT	
					aggr/	grain 1		grain 2				mantle			grain 1		grain 2			enve-	aggr/	relict
	core	core	core	rim	grt	core	rim	core	rim	core	rim	on spl	core	rim	core	rim	core	rim	core	lope	cpx	near spl
SiO_2	54·91	54·76	53·45	52·82	52·13	0·04	0·06	0·04	0·02	0·02	—	37·03	22·54	22·83	3·02	2·99	2·81	2·84	60·20	60·86	40·74	40·08
TiO_2	—	—	0·04	0·03	0·03	—	—	0·02	—	0·02	0·01	—	—	—	0·06	0·09	0·64	0·88			0·02	0·03
V_2O_3						0·03	0·02	0·01	—													
Al_2O_3	4·19	4·01	7·88	10·23	9·68	65·49	65·54	65·88	66·13	99·21	99·05	62·59	76·88	76·94	83·83	83·88	83·37	83·54	25·63	24·80	22·44	22·81
Cr_2O_3	0·05	—	—	0·03	0·02	0·62	0·63	0·98	1·06	0·03	0·08	0·21	0·26	0·37	0·10	0·24	0·13	0·11			0·00	0·03
FeO_t	3·31	3·11	3·54	2·86	3·12	14·59	14·67	13·66	13·41	0·29	0·43	0·28	0·38	0·42	2·38	2·31	2·47	2·28	0·01	0·04	14·36	14·41
MnO	—	—	—	0·01	0·05	0·03	0·01	0·02	0·05	—	0·02	—	0·02	0·02	0·00	0·03	0·00	0·00			0·20	0·20
NiO	0·20	0·22	0·12	0·12	0·15	2·15	2·21	1·96	1·98	0·02	0·01	—	—	0·05							0·00	0·07
ZnO						1·69	1·68	2·07	2·11						0·25	0·22	0·19	0·25				
MgO	14·31	14·24	11·95	11·24	12·03	16·17	16·09	16·18	16·19	—	—	—	0·05	0·01	1·51	1·51	1·59	1·68			11·98	11·45
CaO	21·57	21·68	19·48	19·30	19·69	—	—	0·02	—	0·01	0·02	0·03	0·01	0·05	8·43	8·45	8·38	8·43	6·89	6·23	10·38	11·45
SrO																			0·04	0·03		
BaO																			—	0·02		
Na_2O	2·01	2·00	3·07	3·38	3·04	0·05	0·06	0·05	0·07	0·01	—	—	—	—	—	—	0·02	0·02	7·55	7·99	0·03	0·01
K_2O	—	—	—	0·02	0·00	—	0·02	—	0·01	0·01	—	0·01	0·02	0·01	—	—	0·01	0·01	0·39	0·42	0·01	0·01
Total	100·54	100·02	99·51	100·04	99·94	100·86	100·98	100·87	101·02	99·61	99·62	100·14	100·16	100·70	99·60	99·73	99·61	100·05	100·72	100·38	100·14	100·52
Si	1·977	1·982	1·937	1·897	1·882	0·001	0·002	0·001	0·000	0·000	0·000	0·999	1·188	1·198	0·342	0·338	0·318	0·320	2·665	2·700	3·011	2·965
Ti	0·000	0·000	0·001	0·001	0·001	0·000	0·000	0·000	0·000	0·000	0·000	0·000	0·000	0·000	0·005	0·008	0·055	0·075			0·001	0·002
V						0·001	0·000	0·000	0·000													
Al	0·178	0·171	0·336	0·433	0·412	1·977	1·977	1·985	1·988	1·994	1·992	1·990	4·777	4·761	11·180	11·173	11·132	11·104	1·337	1·297	1·955	1·989
Cr	0·001	0·000	0·000	0·001	0·001	0·012	0·013	0·020	0·021	0·000	0·001	0·004	0·011	0·016	0·009	0·021	0·012	0·010			0·000	0·002
Fe^{3+}					0·000	0·011	0·011	0·000	0·000	0·004	0·006	0·006	0·017	0·018					0·000	0·001		
Fe^{2+}	0·100	0·094	0·107	0·086	0·094	0·302	0·303	0·292	0·286	0·000	0·000	0·000	0·000	0·000	0·225	0·218	0·234	0·215	0·000	0·000	0·887	0·891
Mn	0·000	0·000	0·000	0·000	0·001	0·001	0·000	0·000	0·001		0·000	0·000	0·001	0·001	0·000	0·003	0·000	0·000			0·012	0·012
Ni	0·006	0·006	0·003	0·003	0·004	0·044	0·045	0·040	0·041	0·000	0·000	0·000	0·000	0·002							0·000	0·004
Zn						0·032	0·032	0·039	0·040						0·021	0·018	0·016	0·021				
Mg	0·768	0·769	0·645	0·602	0·648	0·618	0·614	0·617	0·616	0·000	0·000	0·000	0·004	0·001	0·255	0·254	0·269	0·282			1·320	1·263
Ca	0·832	0·841	0·756	0·743	0·762	0·000	0·000	0·000	0·000	0·000	0·000	0·001	0·000	0·002	1·022	1·023	1·017	1·019	0·327	0·296	0·822	0·908
Sr																			0·001	0·001		
Ba																			0·000	0·000		
Na	0·140	0·140	0·216	0·235	0·213	0·002	0·003	0·002	0·004	0·000	0·000	0·000	0·000	0·000	0·000	0·000	0·004	0·004	0·648	0·688	0·004	0·001
K	0·000	0·000	0·000	0·001	0·000	0·000	0·001	0·000	0·000	0·000	0·000	0·000	0·001	0·001	0·000	0·000	0·001	0·001	0·022	0·024	0·001	0·000
Sum	4·003	4·003	4·002	4·002	4·017	3·000	3·000	2·998	2·997	2·000	2·000	3·001	6·000	6·000	13·059	13·057	13·058	13·051	5·001	5·007	8·013	8·037
Mg-no.	88·5	89·1	85·8	87·5	87·3	67·2	67·0	67·9	68·3												59·8	58·6
Al^{IV}	0·020	0·016	0·061	0·100	0·101																	
Al^{VI}	0·159	0·156	0·275	0·333	0·311																	

Mg-number = $100 \times Mg/(Mg + Fe^{2+})$. —, not detected.

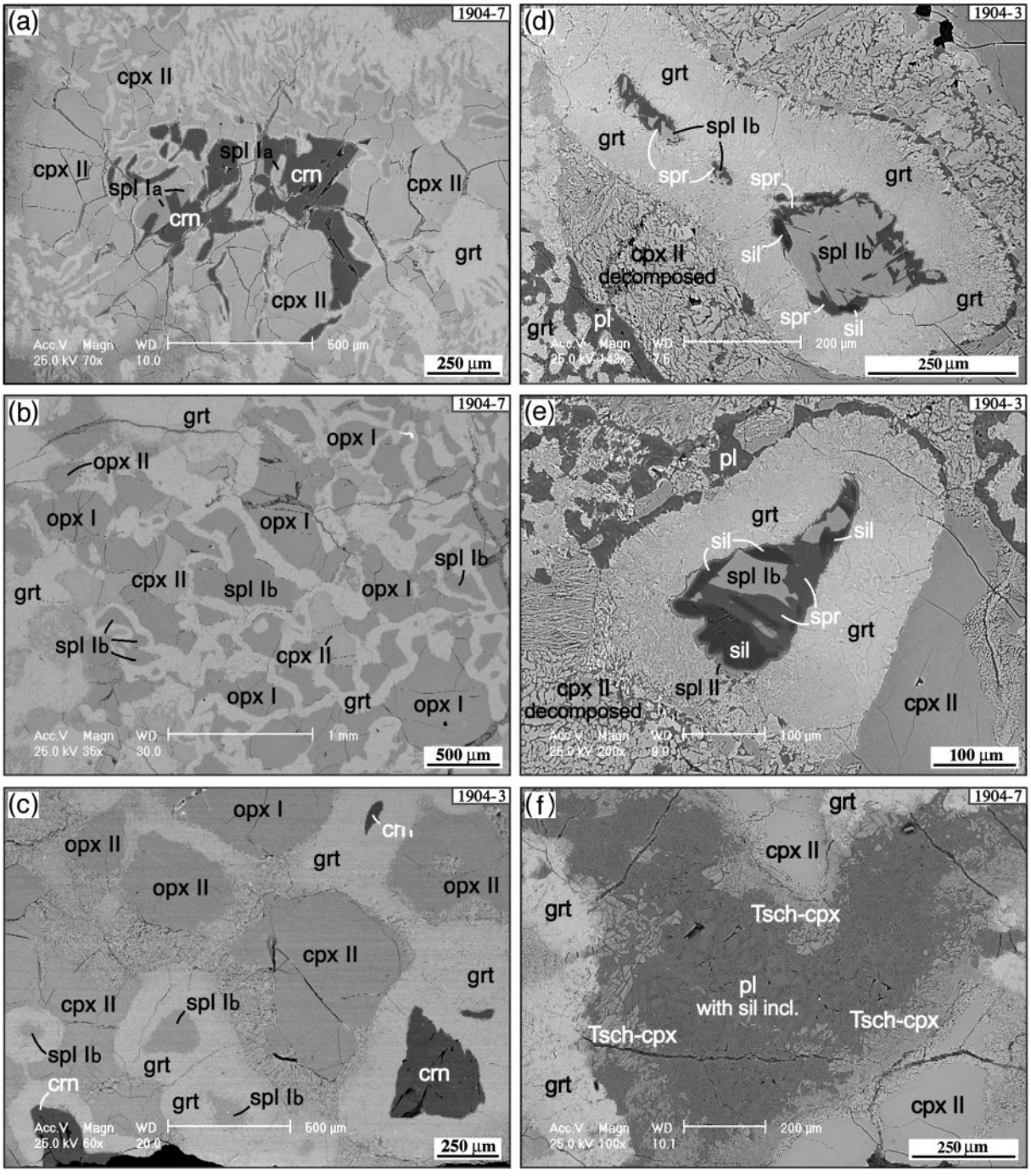

Fig. 3. Back-scattered electron images illustrating different generations of the major mineral phases and important reaction domains in Mg–Al granulites. (a) Spinel Ia partially replaced by corundum and clinopyroxene and resorbed by garnet (domain A1). (b) Coarse-grained symplectites of orthopyroxene, clinopyroxene and spinel resorbed by garnet (domain A2). (c) Coarse-grained aggregate of orthopyroxene, clinopyroxene, spinel and corundum resorbed by garnet (domain A2). (d, e) Sapphirine–sillimanite–garnet coronas around spinel I (domain B). (f) Clusters of Tschermak-rich clinopyroxene (domain D). (For further details, see text.)

rocks are characterized by various types of reaction domains:

(A) worm-like clusters of clinopyroxene and corundum rimming and often completely replacing spinel (A1, Fig. 3a) and coarse-grained to worm-like aggregates of orthopyroxene, clinopyroxene and spinel often accompanied by corundum (A2, Fig. 3b and c);

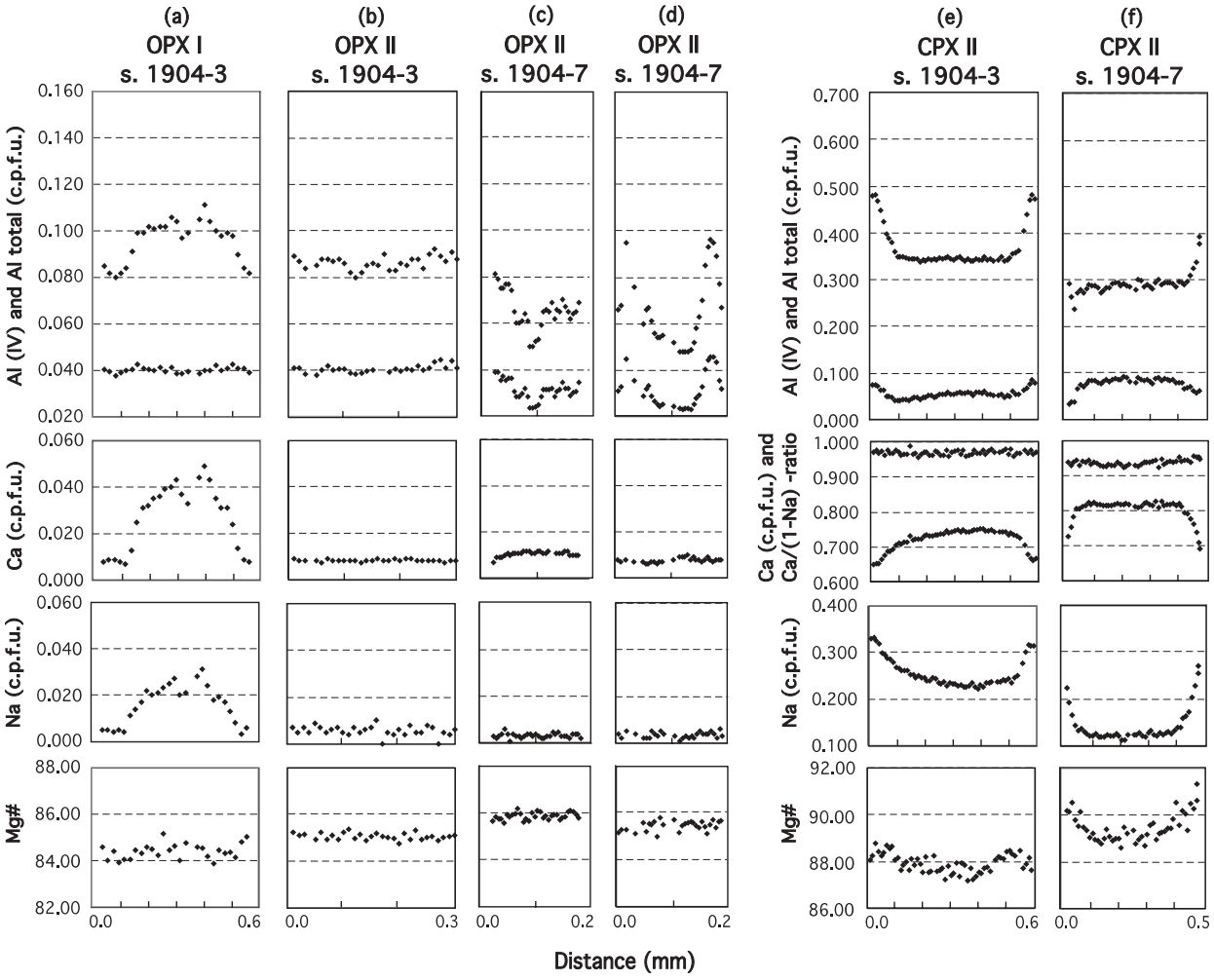

Fig. 4. Zoning patterns of pyroxenes in Mg–Al granulites. (For further explanation, see text.)

(B) sapphirine–sillimanite–garnet coronas on spinel (Fig. 3d and e);

(C) garnet developed at the expense of all mafic phases and forming 'flaky' garnet–plagioclase and massive garnet–clinopyroxene aggregates after plagioclase (Figs 2a and b and 3a–e);

(D) clusters of Tschermak-rich clinopyroxene intergrown with sillimanite and embedded in plagioclase (Fig. 3f).

Orthopyroxene occurs in two generations. Opx I forms large, often elongated xenomorphic grains (Fig. 2a and b). It is exsolved and contains abundant microlamellae of clinopyroxene visible in high-magnification backscattered electron images only. In specimen 1904-7, Opx I is often deformed. It may show undulose extinction and sometimes initial recrystallization. Analysed with a defocused beam, Opx I shows a pronounced decrease in Ca coupled with a moderate decrease in Al towards the rim (Fig. 4a). The Mg-number [$= Mg/(Mg + Fe_{tot})$] remains unchanged. Opx II occurs in two subtypes. The first subtype is common in both specimens (Fig. 2a and b). It occurs as rather small, more or less isometric grains with no deformation, recrystallization or exsolution. The second subtype is found in specimen 1904-7 only. It forms aggregates of small strain-free grains apparently produced by recrystallization of Opx I. These aggregates may be rather large and are always corroded by thin rims of clinopyroxene. All transitions in the degree of exsolution from large exsolved grains of Opx I to relatively small exsolution-free grains of Opx II may be found. Opx II in specimen 1904-3 is nearly homogeneous in all elements (Fig. 4b). In specimen 1904-7, the Al content in Opx II either steadily increases from the core rimwards (Fig. 4c) or increases and then again decreases within the rim (Fig. 4e). The Ca content may slightly decrease rimwards (Fig. 4c). The Mg-numbers of orthopyroxene range from 84·0 to 86·0. CaO in Opx I, analysed with a defocused beam, reaches 1·2–1·5 wt %, whereas the

CaO content in Opx II is much lower (0·16–0·24 wt %; Table 2).

Clinopyroxene forms two (1904-3) or three (1904-7) generations. The first generation is in equilibrium with Opx II and will therefore be further referred to as Cpx II (Fig. 2a and b). Cpx II grains occur as part of reaction domains A (Fig. 3a–c). They do not show any exsolution effects, with the larger grains showing chemically homogeneous cores. Towards the rim, an increase in Al, Na and Mg-number and a decrease in Ca are observed (Fig. 4e and f). The zonation is systematic and regular in specimen 1904-3, where all grains of Cpx II display very similar profiles (Fig. 4e). In specimen 1904-7, however, the zonation is irregular (Fig. 4f). The rim contents of Al vary over a wide range from profile to profile. Cpx III occurs in reaction domains C (Fig. 2a) or as mantles on Opx II, and is compositionally similar to the rims or intermediate zones of Cpx II grains (Table 2). Cpx IV is unusual. Found in specimen 1904-7 only, it forms part of reaction domains D (Fig. 3f). It is extremely rich in Tschermak components and has 18–23 wt % Al_2O_3 (Table 2). The Mg-numbers of clinopyroxene range from 85·9 to 92·2. CaO ranges from 17·0 to 21·6 wt % (Table 2).

Spinel forms two textural generations. Spl I is common and occurs as large, more or less isometric grains in reaction domains A and B (Fig. 3a–c). Two subtypes of Spl I can be distinguished. Spl Ia is present in specimen 1904-7 only, where it forms individual grains enclosed in plagioclase and partially or completely replaced by clinopyroxene and corundum (reaction domain A1, Fig. 3a). It does not show any evidence for earlier coexistence with ortho- and clinopyroxene. Spl Ib is ubiquitous and occurs as part of reaction domains A2 (Spl + Opx + Cpx ± Crn, Fig. 3b and c) and B (Spl + Spr + Sil + Grt, Fig. 3d and e) in both specimens. Chemically, the two subtypes of spinel are not well distinguishable. Cr tends to concentrate in Spl Ia (0·30–0·77 wt % Cr_2O_3 at 0·90–1·30 wt % NiO), whereas Ni preferably concentrates in Spl Ib (up to 1·74 wt % NiO, but at 0·10–0·35 wt % Cr_2O_3). The Mg-number ranges from 71·8 to 76·6 (Table 1). Spl I is not zoned but some grains may show a decrease in the Mg-number restricted to the outermost 10–20 μm. Spl II forms very thin rims on sillimanite in some of reaction domains B (Fig. 3d and e). It cannot be analysed, because of its small size.

Corundum forms worm-like intergrowths with clinopyroxene and platy aggregates with spinel in reaction domains A1 (Fig. 3a), as well as large individual grains in reaction domains A2 (Figs 2a and 3c). Corundum contains up to 0·50 wt % Fe_2O_3 and 0·16 wt % Cr_2O_3 (Table 2). Some grains are slightly zoned whereby Cr and Fe increase and Al decreases rimwards.

Plagioclase forms large grains and granular aggregates with frequent sillimanite inclusions. In the rim parts of such aggregates, it is often intimately intergrown with garnet forming 'flaky' Grt–Pl aggregates. Plagioclase also occurs as thin envelopes mimicking the borders of some Cpx II grains. Plagioclase is relatively Na-rich ($An_{21–16}$ for 1904-3; $An_{40–30}$ for 1904-7; Table 2). It may show some enrichment in Na in the envelopes around clinopyroxene II (Table 2).

Garnet replaces almost all other minerals, forming a network-like structure around pyroxene, spinel and corundum grains, 'flaky' aggregates with plagioclase and massive aggregates with Cpx III (Figs 2a and b and 3a–e). As garnet itself is normally replaced by kelyphite, only rare relicts are available for analysis. The Mg-number ranges from 62·6 to 70·1 and CaO from 4·2 to 6·0 wt % (Table 2).

Sapphirine forms small platy inclusions in the outermost zones of spinel I grains or rims spinel I in reaction domains B (Fig. 3d and e). In the latter case, sapphirine apparently resorbs spinel and, in turn, is being replaced by sillimanite or directly by garnet. Sapphirine compositions are close to the ideal composition $7(Fe,Mg)O \times 9(Fe,Al,Cr)_2O_3 \times 3SiO_2$ (Table 2). NiO reaches 0·50 wt % and is the only minor component.

Sillimanite rims sapphirine and spinel in reaction domains B (Fig. 3d and e) and forms frequent needle-like inclusions in plagioclase (Figs 2b and 3f). If associated with spinel and sapphirine, sillimanite tends to replace spinel, always replaces sapphirine and, in turn, is resorbed by garnet. Sillimanite hosted in plagioclase appears to be in textural equilibrium with the latter. Fe_2O_3 contents are <0·65 wt % (Table 2).

Ca–Al hibonite-bearing granulites

The three studied samples (1904-1, 1904-9, 1906-2) are very similar to each other. Xenolith 1904-1 is relatively coarse-grained (plagioclase grains reach 3–4 mm, mafic minerals are smaller in size) and banded. Xenoliths 1904-9 and 1906-2 are finer grained and homogeneous. Specimen 1906-2 is more mafic compared with the others. Major minerals in all samples are clinopyroxene and plagioclase, while corundum and garnet are essential (~10–15 vol. % each) and quartz, spinel and sillimanite subordinate (5–7 vol. %). In addition, sapphirine in sample 1904-1 and hibonite in samples 1904-1 and 1904-9 occur as rare accessories. Mullite is very rare. It is encountered in one specimen (1904-9), and only in three grains.

Textures are characterized by felsic and mafic domains. The felsic domains consist of plagioclase and the mafic domains are dominated by clinopyroxene, corundum, garnet, spinel, sillimanite and quartz (Fig. 2c). Both domains are normally separated by a fine-grained corona that consists of garnet and recrystallized plagioclase, grading locally, as in the Mg–Al granulites, into a

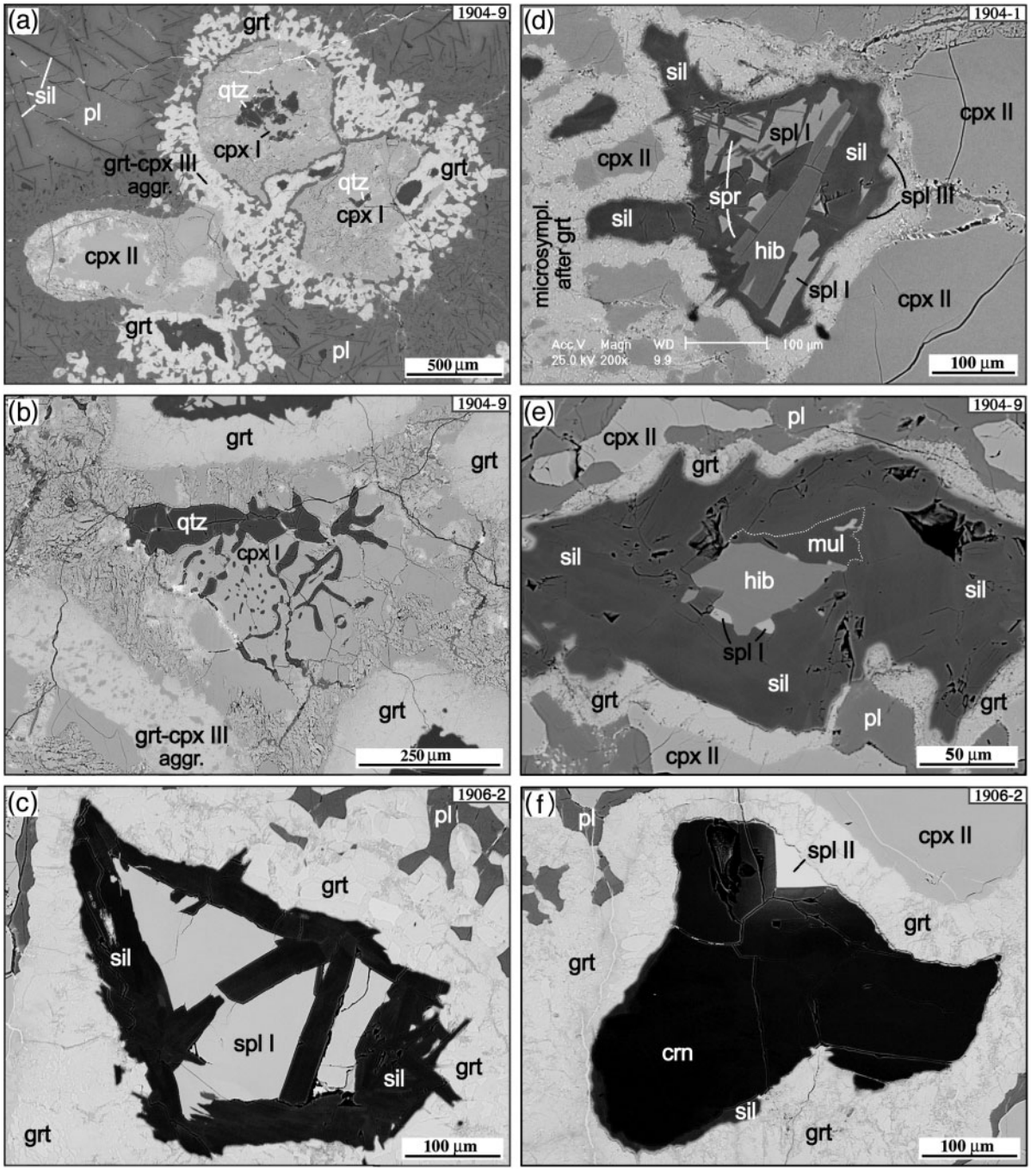

Fig. 5. Back-scattered electron images demonstrating the different mineral generations and important reaction domains in Ca–Al granulites. (a, b) Large complex grains of clinopyroxene I with quartz in the cores. (c) Spinel I intergrown with and rimmed by sillimanite. (d) Aggregate of hibonite, spinel, sapphirine and sillimanite partially resorbed by garnet. (e) Aggregate of hibonite, spinel, mullite and sillimanite partially replaced by garnet. (f) Corundum aggregated with spinel II, partially rimmed by sillimanite and strongly replaced by garnet. (For further explanation, see text.)

massive zone of intimately intergrown micrograins of garnet and clinopyroxene (Figs 2c and 5a and b).

Clinopyroxene can be divided into three generations. Cpx I occurs in close association with quartz. Together, they form granular cores of large complex clinopyroxene grains (Fig. 5a and b). Typically, such cores contain either one to several large (0·2–0·3 mm) or 10–20 small (<0·1 mm) drop-like inclusions of quartz with different optical orientations. Worm-like intergrowths of quartz and Cpx I may occur as well. Apart from this texture,

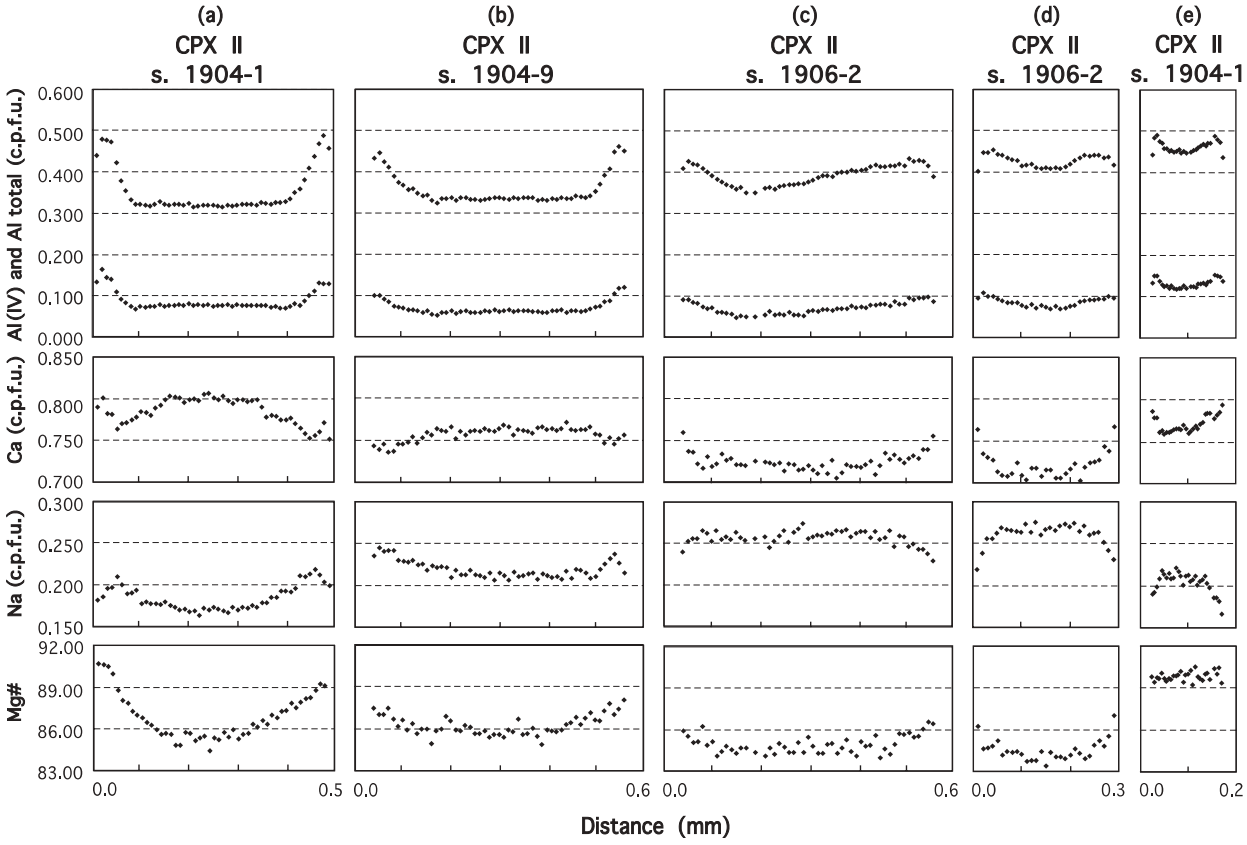

Fig. 6. Zoning patterns of clinopyroxenes in Ca–Al granulites. (For further explanation, see text.)

the rocks are devoid of quartz. The core is always mantled by an outer zone of clinopyroxene that lacks quartz. Normally, the whole grain is embedded in plagioclase. Cpx II forms smaller grains that do not have quartz. Cpx III forms very small (<10 μm) grains intergrown and texturally equilibrated with garnet in the massive fine grained Grt–Cpx zones developed after plagioclase (Fig. 2c).

In general, clinopyroxene is characterized by moderate to high Mg-number (86·3–91·2 in Cpx I, 83·6–90·7 in Cpx II and III). CaO ranges from 18·05 to 21·68 wt % (Table 3). Chemically, Cpx I is easily distinguishable from Cpx II and III. It is more magnesian than Cpx II, more Ca-rich, less aluminous and much less tschermakitic than Cpx II and III (Table 3). Cpx II is zoned (Fig. 6). If no inclusions are present, the core parts of the largest grains display plateaux in Al (Fig. 6a and b). Closer to the rims, the Al content increases and then always slightly decreases again within the outermost 10 μm. The Na zonation mimics that of Al but is less extreme; Ca shows the inverse pattern to Na (Fig. 6). The Mg-number increases rimwards, sometimes with a slight tendency to decrease again within the outermost rim (Fig. 6). In smaller grains, Cpx II shows the same style of zonation, but with no plateau (Fig. 6c–e). Cpx III has a composition intermediate between the core and the rim zones of Cpx II (Table 3).

Plagioclase forms large isometric or elongated grains with abundant needle-like inclusions of sillimanite and late inclusion-free envelope-like zones mimicking the borders of clinopyroxene II in contact with the 'flaky' Grt–Pl or massive Grt–Cpx aggregates (Figs 2c and 5a). As an exception, plagioclase occurs as amoeboidal inclusions in clinopyroxene. Plagioclase is Na-rich ($An_{39–34}$ for 1904-1; $An_{35–32}$ for 1904-9; $An_{31–26}$ for 1906-2). It is slightly inhomogeneous and shows a tendency towards higher Ab in the envelopes (Table 3).

Corundum forms grains of variable shape. It is always closely associated with clinopyroxene and often occurs as inclusions in the latter (Fig. 2c). Isolated grains of corundum are Cr-poor and almost unzoned. Rare corundum grains intergrown with Spl II demonstrate strong chemical zonation towards Spl II: the content of Cr_2O_3 reaches ~7·0 wt %, whereas the Al content decreases (Table 3).

Garnet replaces almost all other minerals and does not form independent grains. Most garnet is developed at the expense of corundum and plagioclase. As a rule, garnet is

altered into kelyphite, only rare relics are preserved. The Mg-number ranges from 58·6 to 65·5, and CaO content varies from 7·90 to 11·45 wt % (Table 3).

Spinel can be subdivided into three generations. Spl I is common. It forms relatively large grains always associated with sillimanite, sometimes also with sapphirine, hibonite or mullite. The textural relationships between Spl I, Sil and other minerals are not easily discernible. Almost all grains of Spl I are completely mantled by platy crystals of sillimanite (Fig. 5c and d). Besides that, sillimanite tends to separate spinel into individual blocks, and all transitional forms from single grains of Spl I with a Sil mantle to well-developed mosaic intergrowths of Spl I and Sil are observed (e.g. Fig. 5c). Some of these aggregates show clear textural indications of sillimanite replacing spinel. In others, these minerals seem to be in textural equilibrium. Sapphirine, mullite and/or hibonite, if present, occur in the core areas of the Spl–Sil aggregates (Fig. 5d and e). Of these minerals, only mullite apparently resorbs spinel (Fig. 5e). Hibonite shows linear contacts with spinel with no clear indications of resorption, although spinel often rims hibonite and not vice versa. The aggregates are always corroded by garnet (Fig. 5c–e). Except for one case of direct contact with spinel, garnet resorbs only the outer sillimanite mantle, but not the inner mineral assemblage (Fig. 5c–e). In thin section, the described aggregates are always closely associated with Cpx I and II (Figs 2c and Fig. 5d and e).

Spinel II is rare. It forms small grains localized directly at the rims of the larger corundum grains, or penetrating corundum from the rim inwards (Fig. 5f). Late spinel III occurs as very thin mantles picking out borders of corundum and sillimanite in the various aggregates (e.g. Fig. 5d).

Individual Spl I grains are nearly homogeneous but they show considerable inter-grain variations in Cr_2O_3 contents and Mg-number, depending on their textural position (Table 3). Cr_2O_3 typically ranges from 0·3 to 6·0 wt %, but is lower (0·3–2·7 wt %) in Spl I associated with hibonite and much higher (up to 22 wt %) in some of the Spl I–Sil aggregates. Mg-number ranges from 66·5 to 70·9 (Table 3). NiO and ZnO are generally high (1·1–2·3 and 1·0–2·6 wt %, respectively). Spinel II is also nearly homogeneous in individual grains. It is extremely rich in Cr (33–40 wt % Cr_2O_3) and has lower NiO contents and Mg-number than Spl I (Fig. 7; Table 3). The composition of spinel III is not easily measurable because of small grain size.

Sillimanite forms platy aggregates with spinel I (Fig. 5c), outer zones on spinel I and its aggregates with hibonite, mullite and sapphirine (Fig. 5d and e), as well as frequent needle-like inclusions in plagioclase (e.g. Fig. 5a). In the aggregates, sillimanite apparently resorbs hibonite, may resorb spinel I, sapphirine and mullite (Fig. 5d and e) and, in turn, is resorbed by garnet. Sillimanite shows a spectrum of compositions from nearly ideal in most cases to Cr-rich (up to ~2·0 wt % Cr_2O_3) in contact with Cr-rich Spl I. Fe_2O_3 may amount to 0·65 wt % (Table 3).

Sapphirine occurs as a rare accessory phase and is identified with confidence in specimen 1904-1 only. In specimen 1906-2, it may be present as micro-relicts enclosed in sillimanite in the outer parts of Spl–Sil aggregates, but the grains are too small to be analysed by electron microprobe. Sapphirine in specimen 1904-1 is closely associated with spinel, hibonite and sillimanite (e.g. Fig. 5d). It may show straight borders with Spl I with no indications of resorption, but more often it resorbs Spl I. In turn, it is always resorbed by sillimanite, and in some cases directly by garnet. The analysed sapphirine is close to the ideal composition $7(Fe,Mg)O \times 9(Fe,Al,Cr)_2O_3 \times 3SiO_2$. Cr_2O_3 may reach 1·12 wt %, and NiO 0·47 wt % (Table 3).

Mullite occurs in specimen 1904-9 only. It is found in the cores of three spinel–hibonite–sillimanite aggregates, one of which is shown in Fig. 5e. Mullite apparently resorbs hibonite and spinel I and, in turn, is replaced by sillimanite. Chemically, it belongs to the 2:1 type ($2Al_2O_3$:$1SiO_2$). In the mullite solid solution series $Al_{4+2x}Si_{2-2x}O_{10-x}$ (Cameron, 1977), it is characterized by $x \approx 0{\cdot}40$ (Table 3). The mullite is nearly homogeneous. It may contain limited amounts of Cr_2O_3 and FeO_t (<0·50 wt % each; see Table 3).

Hibonite occurs as accessory phase in xenoliths 1904-1 and 1904-9. Its absence in xenolith 1906-2 may be due to the relative depletion of its bulk chemical composition in Al and Ca compared with xenoliths 1904-1 and 1904-9 (see Table 1). Hibonite forms small isometric or elongated, often complexly indented grains intergrown with spinel I in the cores of complex corona textures made of hibonite, spinel, mullite, sapphirine and sillimanite (Fig. 5d and e). Neither hibonite nor spinel and sapphirine replaces each other. At the same time, the petrographic relationships of hibonite with spinel and sapphirine point to early crystallization of hibonite, as both spinel and sapphirine tend to localize on the border of hibonite grains, while hibonite never rims either spinel or sapphirine (Fig. 5d and e). Mullite, when present, apparently resorbs hibonite, just as sillimanite does (Fig. 5e).

Chemically, the studied hibonite is close to the ideal formula $Ca(Al,Ti,Si,Mg,Fe^{2+})_{12}O_{19}$. Ca, Al, Si, Mg and Fe contents vary in a narrow range. SiO_2 ranges from 2·32 to 3·10 wt %. Some TiO_2 is always present (0·05–0·74 wt % in specimen 1904-1, 0·26–2·29 wt % in specimen 1904-9). Significant intergrain variations and a systematic rimwards increase in Ti are also common. Cr_2O_3 ranges from 0·03 to 0·52 wt %, and ZnO does not exceed 0·25 wt % (Table 3). Ca contents vary from 1·016 to 1·048 c.p.f.u. and are somewhat in excess

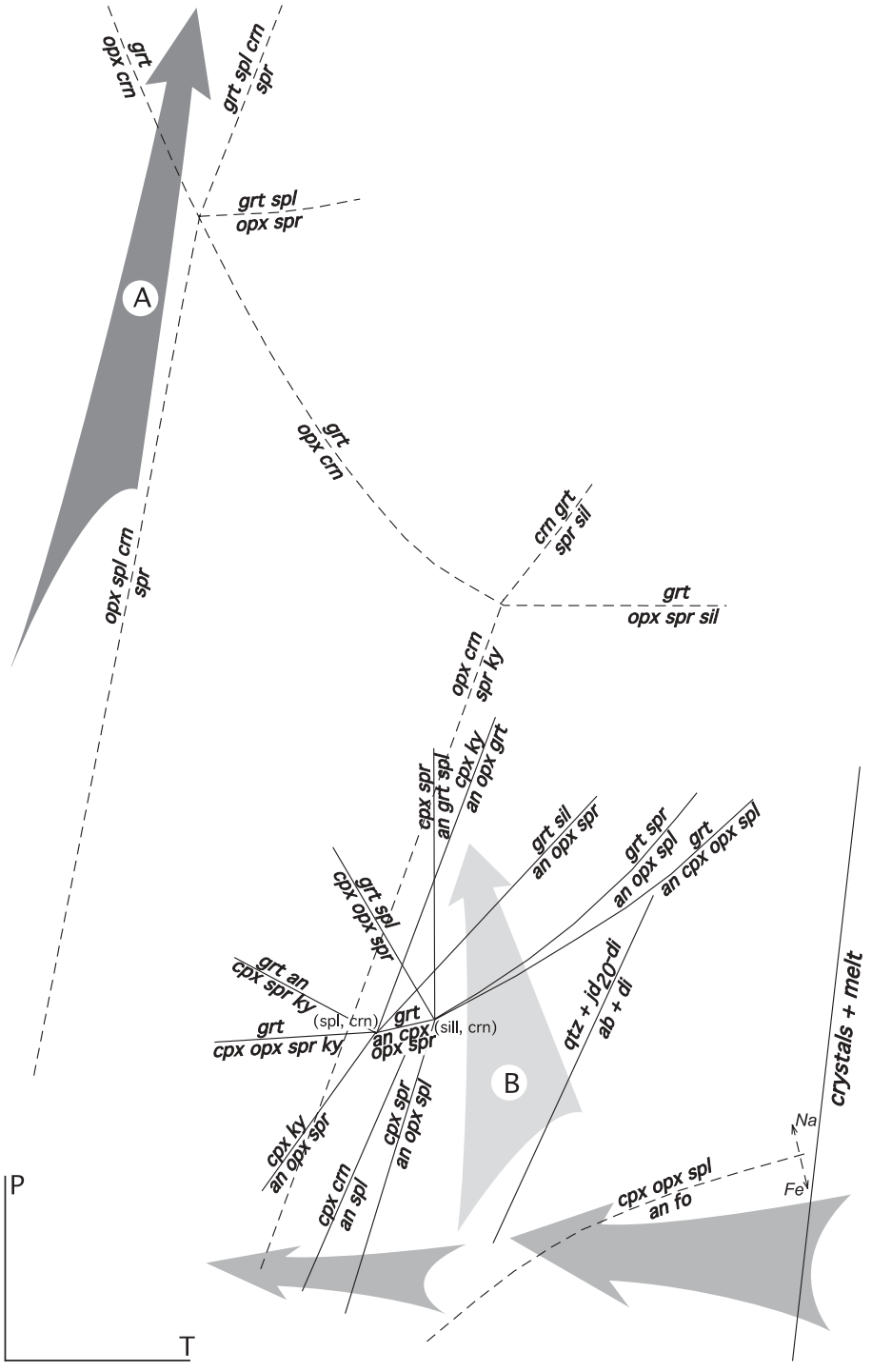

Fig. 7. Qualitative pressure–temperature diagram showing the inferred *P–T* path of the studied granulite xenoliths [Schreinemakers analysis for the CMAS and MAS systems after Christy (1989) and Ouzegane *et al.* (2003), respectively. Also shown are the reactions Spl + An = Crn + Di from Morishita & Arai (2001) and Ab + Cpx = Qtz + Jd_{20}–Cpx from Kushiro (1969)].

compared with the ideal stoichiometry of hibonite. An excess of Ca has been found in both terrestrial (e.g. Maaskant *et al.*, 1980) and meteoritic (e.g. Keil & Fuchs, 1971; MacDougall, 1979) hibonite and is common for this mineral. This indicates that an exchange of (Mg,Fe^{2+}) and Ca in site A of the hibonite structure is unlikely. At the same time, the classical substitution (Ti,Si) + (Mg,Fe^{2+}) ↔ 2(Al,Cr) in site B (e.g. Burns &

Burns, 1984) and the common exchange Ti ↔ 2(Mg,Fe^{2+}) were operative (Ulianov *et al.*, 2005). The studied hibonite is very poor in REE (ΣREE from 1·5 to ~30 μg/g) with positive Eu anomalies and variable enrichment in LREE and very low abundances (<1–2 μg/g) of Nb, Ta, Zr, Hf and Th (Ulianov *et al.*, 2005).

PRE-METAMORPHIC VS METAMORPHIC MINERAL ASSEMBLAGES

The studied xenoliths are considered to have undergone nearly complete subsolidus recrystallization. Although their CIPW normative compositions are troctolitic, modal olivine is absent. It seems to have completely reacted out during subsolidus cooling, as discussed below. The plagioclase grains actually present show indications of metamorphic re-equilibration and thus do not represent igneous relicts, texturally or compositionally.

In the Mg–Al sapphirine-bearing granulites, the only potential igneous relicts are the largest grains of orthopyroxene (Opx I), of which the reintegrated composition is very rich in calcium and aluminum (Table 2), and possibly a minor part of spinel texturally independent of pyroxenes (Spl Ia). Spinel Ia compositions, however, re-equilibrated under subsolidus conditions and are almost indistinguishable from those of metamorphic spinel Ib (see the section on 'Textures and mineral compositions'). Sapphirine never forms individual grains and is found only as a constituent of the complex corona textures developed around the grains of Spl I, most of which are metamorphic in origin (see the section on 'Metamorphic reactions'). Therefore, we do not interpret sapphirine as magmatic, although it may be a liquidus phase in basic Al-rich bulk compositions (Liu & Presnall, 1990, 2000). Corundum appears texturally equilibrated with metamorphic spinel and pyroxenes (Fig. 3c; see the section on 'Metamorphic reactions') and is hence not considered to be igneous even though it may also be a liquidus phase in basic Al-rich bulk compositions (Liu & Presnall, 1990, 2000). Sillimanite and garnet form only reaction rims and are clearly of metamorphic origin.

In the Ca–Al hibonite-bearing granulites, hibonite and some spinel are the only phases that could be igneous relicts; hibonite in terms of composition and textures, and spinel only texturally. The metamorphic transformation of the initial troctolitic assemblage olivine + plagioclase on cooling must have formed pyroxenes and spinel, as in the Mg–Al granulites (see the section on 'Metamorphic reactions'). Spinel grains intergrown with or rimmed by sillimanite are common in the studied specimens, although some of them may texturally represent relicts of the igneous stage. When hibonite is present together with spinel in such aggregates, spinel grains tend to localize on the border of hibonite grains and sometimes rim hibonite, whereas hibonite never rims spinel (see Fig. 5d and e, and the section on 'Textures and mineral compositions'). Therefore, hibonite can be considered as the earliest mineral of the reaction sequence most likely to represent an igneous relict. The latter hypothesis is confirmed by experiments that show hibonite to be a liquidus phase in experimental systems relevant to Ca,Al-rich inclusions in chondrite meteorites (Drake & Boynton, 1988; Beckett & Stolper, 1994; Kennedy *et al.*, 1994). Some hibonites from the liquidus experiments are markedly enriched in silica (up to 1·7 wt %) despite the strong silica undersaturation of the coexisting melt (Beckett & Stolper, 1994). This suggests that high silica contents (as in the studied hibonites; see Table 2) may be characteristic of igneous hibonite.

Hibonite in the studied xenoliths is characterized by significant chemical variations, particularly in Ti and REE. Hibonites with very low Ti contents may retain their pristine (igneous) chemical composition, whereas high-Ti hibonites were apparently re-equilibrated during metamorphism (Ulianov *et al.*, 2005).

THERMOBAROMETRIC CONSTRAINTS

In the Mg–Al sapphirine-bearing granulites, quartz is completely absent and thus no geobarometers based on Px–Pl–Grt–Qtz assemblages can be used. In the Ca–Al hibonite-bearing granulites, quartz is not equilibrated with garnet and plagioclase, thus excluding the application of Grt–An–Cpx–Qtz or Grt–An–Sil–Qtz geobarometers. Barometry based on the reaction Spl + Qtz = Grt + Sil (Bohlen *et al.*, 1986; Nichols *et al.*, 1992) is hampered by the lack of data on the equilibrium composition of garnet in the course of early metamorphism, to which this reaction is relevant. Given the presence of sillimanite and the absence of kyanite or textures indicating growth of sillimanite at the expense of kyanite in the studied xenoliths, the P–T evolution of the granulites seems limited to the sillimanite stability field. We thus fixed a maximum pressure of 8 kbar for all temperature calculations.

For the Mg–Al granulite xenoliths, we calculated temperatures using the cores of Opx I with the exsolved lamellae of Cpx. We obtained estimates of 1090 and 1135°C with the Ca-in-Opx thermometer of Brey & Köhler (1990) (see Table 4). These temperatures probably correspond to an early stage of subsolidus cooling rather than to the magmatic crystallization of the protolith because the original composition of Opx I was modified by diffusion owing to mineral re-equilibration on cooling. For the latest stage of equilibration recorded in the pyroxene rims and in the aggregates of Cpx III and

Table 4: P–T *estimates for studied granulites*

	Mg–Al sapphirine granulites		Ca–Al hibonite granulites		
	1904-7	1904-3	1904-1	1904-9	1906-2
Reintegrated core compositions of opx I in two-px granulites; P is fixed at 8 kbar					
T Ca-in-opx (Brey & Köhler, 1990)	1135	1090			
Rim compositions of px II; px III; P is fixed at 8 kbar					
T two-px solvus (Brey & Köhler, 1990)	730 (26)	585 (24)			
T two-px solvus (Wells, 1977)	753 (27)	688 (22)			
T Ca-in-opx (Brey & Köhler, 1990)	714 (28)	737 (29)			
T opx–grt (Harley, 1984)	784 (37)	740 (27)			
T grt–cpx (Krogh Ravna, 2000)	559 (42)	642 (27)	639*	725 (30)	741 (29)
T grt–cpx (Ai, 1994)	514 (41)	616 (30)	635*	731 (33)	730 (31)

Values in parentheses are uncertainties.
*Garnet is completely altered to kelyphite, only one small inclusion in the outer mantle of a Cpx I grain survived.

Grt, the temperature estimates range widely from 514 to 784°C, depending on the geothermometer used (Table 4). Discrepancies between the estimates based on the two-pyroxene solvus and on the Fe–Mg exchange between Grt and Cpx may indicate either unreliability of solvus geothermometry in this range of temperatures, or differences in the diffusivities of Ca, Fe and Mg. In specimen 1904-7, where phases are poorly equilibrated in general, the discrepancies are especially pronounced.

For the Ca–Al granulite xenoliths, temperatures may be evaluated with confidence only for the latest stage of equilibration recorded in the pyroxene rims and in the aggregates of Cpx III and Grt. The estimates from two conventional Fe–Mg Cpx–Grt geothermometers (Ai, 1994; Krogh Ravna, 2000) are shown in Table 4. Almost no discrepancies between these two geothermometers are observed. Specimens 1904-9 and 1906-2 are 'hotter' (725–741°C) than specimen 1904-1 (635–639°C).

METAMORPHIC REACTIONS IN THE Mg–Al SAPPHIRINE-BEARING GRANULITES

The major metamorphic features of these rocks that have to be explained are reaction domains A and B as well as the ubiquitous formation of garnet (see the section on 'Textures and mineral compositions').

Reaction domain A1: formation of worm-like clusters of Cpx + Crn rimming and often completely replacing Spl (Fig. 3a). Spinel Ia in the cores of the clusters is early and has reacted with enclosing plagioclase. Obviously, the sapphirine- and sillimanite-forming reactions of domain B (described below) could not initiate, because of the absence of adjacent pyroxenes. Instead, the reaction Spl + Pl = Cpx + Crn took place (see Fig. 7). The lack of pyroxenes around Spl Ia grains may also suggest that these grains were not produced by the reaction Ol + Pl = Opx + Cpx + Spl but that they represent earlier, perhaps igneous relicts (see the section on 'Pre-metamorphic vs metamorphic mineral assemblages'). Metamorphic Cpx–Crn aggregates formed by the reaction Spl + Pl = Cpx + Crn have, to our knowledge, not yet been described from localities elsewhere. Assemblages of Spl and Pl formed at the expense of Cpx and Crn are known from mafic rocks within the Horoman Peridotite complex, as described by Morishita & Arai (2001). The reaction Spl + Pl = Cpx + Crn in the CMAS system has been calculated by those workers at ~800°C at the pressures relevant here (8 kbar). In the Mg–Al granulites, this reaction was crossed towards the low-temperature side (Cpx + Crn) upon cooling.

Reaction domain A2: formation of pyroxenes and spinel (± corundum). The coarse-grained, worm-like or symplectitic aggregates of Opx II, Cpx II and Spl Ib (Figs 2a and 3b) are interpreted to have formed at the expense of the primary igneous assemblage olivine + plagioclase. Such Opx–Cpx–Spl textures are well documented from several localities (e.g. Tenthorey *et al.*, 1996; Müntener *et al.*, 2000; Montanini & Tribuzio, 2001). The reaction Ol + Pl = Opx + Cpx + Spl in the CMAS system is univariant and has been determined experimentally by many workers (Kushiro & Yoder, 1966; Herzberg, 1978; Gasparik, 1984*a*). The high-temperature assemblage Ol + Pl is stable at 1250–1300°C at relatively low pressures (~8 kbar; Kushiro & Yoder, 1966). In the Mg–Al granulites, this assemblage was replaced by Opx + Cpx + Spl, probably during cooling after igneous crystallization.

In Fig. 7, this reaction is shown schematically, because iron in natural systems, preferably accommodated by spinel, displaces the reaction to lower pressures, whereas sodium in plagioclase causes the opposite effect, with the additional chemical components making the reaction at least trivariant.

The Opx–Cpx–Spl aggregates may contain corundum forming individual grains (Figs 2a and 3c) and, less frequently, intergrowths with Spl I. Because no indications for the growth of corundum at the expense of pyroxenes or spinel (and vice versa) in these domains are observed, corundum seems to have formed in equilibrium with pyroxenes and spinel. This points to the reaction Ol + Pl = Cpx + Opx + Spl + Crn that replaces Ol + Pl = Cpx + Opx + Spl upon cooling, provided the pressure is relatively low. To our knowledge, this reaction has not been described from experiments or from nature, nor has it been calculated in any grid. It must, however, take place within the stability field of Opx + Crn, which is limited to temperatures below ~850°C at the pressures of interest (~8 kbar) in MAS grids (Gasparik, 2003; Ouzegane *et al.*, 2003; Kelly & Harley, 2004). The feasibility of this reaction for natural systems depends on the bulk chemical composition (e.g. Na and Fe contents) and its variations in local domains of the studied rocks, which affects the stability of the assemblage Cpx + Opx + Spl + Crn in *P–T* space.

Reaction domain B: formation of sapphirine and sillimanite. The sapphirine–sillimanite coronas on spinel I (Fig. 3d and e) occur only in cases where the initial spinel is situated near both plagioclase and pyroxene. The key to understanding this texture is given by Fig. 3d and e. Although spinel I appears strongly resorbed by garnet, both sapphirine and sillimanite are present even on the smallest relicts of Spl I (Fig. 3d). This texture points to the co-crystallization of the assemblages Grt + Spr and Grt + Sil after spinel I, plagioclase and pyroxene. It argues against the formation of only sapphirine and sillimanite after spinel, with subsequent resorption of the resulting Spl–Spr–Sil coronas by garnet. A possible sequence of reactions during cooling, leading to the Spr–Sil–Grt corona textures after spinel, can be inferred from a Schreinemakers analysis in the CMAS system (Christy 1989; Fig. 7) as follows:

$$\text{An} + \text{Cpx} + \text{Opx} + \text{Spl} + \text{Grt} \quad \text{and}$$
$$\text{An} + \text{Opx} + \text{Spl} = \text{Grt} + \text{Spr} \qquad (1)$$

$$\text{An} + \text{Opx} + \text{Spr} = \text{Grt} + \text{Sil}. \qquad (2)$$

Reactions (1), nearly degenerate, probably acted simultaneously and are responsible for sapphirine and garnet, whereas reaction (2) produced sillimanite and garnet once spinel was mantled by sapphirine and garnet. Reaction coronas similar to those described here are known in their fully developed forms only in granulite xenoliths from the Stockdale kimberlite, Kansas (Meyer & Brookins, 1976).

Reaction domain C: formation of garnet. The occurrence of garnet in the corona textures with spinel, sillimanite and sapphirine (Fig. 3d and e) can be satisfactorily explained by the Schreinemakers diagram (Fig. 7), as discussed above. Garnet developed at the expense of corundum (Fig. 2a), can be attributed to the reaction Crn + Opx ± Cpx = Grt. The resorption of pyroxene grains located close to corundum by garnet can also be explained by this reaction. Garnet resorbing pyroxenes and spinel in reaction domains A (Fig. 3b) cannot have formed by the reaction Opx + Cpx + Spl = Grt, as the latter requires additional silica in order to consume spinel. We speculate, therefore, that plagioclase participated in the reaction Opx + Cpx + Spl + Pl = Grt (Gasparik, 1984*a*). The 'flaky' and massive zones of garnet or garnet and clinopyroxene propagating into and resorbing plagioclase (Fig. 2a) may also be explained by this reaction or by Opx + Spl + Pl = Grt + Cpx (Green & Ringwood, 1967) taking place simultaneously to the development of garnet in reaction domains A and B. Similar reaction zones of garnet after spinel, pyroxenes and plagioclase in metamorphosed metabasites have been described from many occurrences of mafic granulites throughout the world (e.g. Griffin, 1971; Irving, 1974; Indares & Rivers, 1995; Attoh, 1998; Indares, 2003), including meta-anorthosites and related rocks of eastern and northeastern Tanzania (Appel, 1996; Appel *et al.*, 1998). Most of the above reactions can easily take place during cooling, either isobaric or concomitant to/followed by compression, although only the garnet-forming reaction Crn + Opx ± Cpx = Grt clearly necessitates compression (Fig. 7).

Although garnet seems generally stable and no textural evidence for its breakdown has been found, in specimen 1904-7 it may have started to decompose to the very end of the reaction path. A possible reaction (Pl + Grt = Cpx + Sil) involves also plagioclase and accounts for the formation of Cpx IV with its exceptional concentrations of Al (reaction domain D). Similar mineral relations are observed in sapphirine-bearing granulites from Stockdale (Meyer & Brookins, 1976).

It is worth stressing the importance of local chemical heterogeneities and additional chemical components in the studied rocks, which control the *P–T* dependence of the described mineral assemblages. For example, the formation of spinel–sillimanite–sapphirine–garnet corona textures in reaction domains B instead of clinopyroxene–corundum aggregates A1 and pyroxene–spinel–garnet aggregates A2 is controlled by the availability of pyroxenes and plagioclase, respectively. Also, in the CMAS system, the reaction Pl + Ol = Cpx + Opx + Spl takes place at a maximum pressure of

~8 kbar at near-solidus temperatures (Kushiro & Yoder, 1966; Gasparik, 1984*a*), but is displaced to lower pressures in Fe-rich compositions. As the granulites are somewhat heterogeneous, the reaction does not take place simultaneously in all reacting domains and, on isobaric cooling, may proceed before the assemblage Crn + Opx + Cpx becomes stable. This appears to define the presence of corundum in domains A2 (see above).

The MAS reaction Opx + Crn = Grt, accounting for the formation of most garnet in the studied specimens, lies at high pressures (>15 kbar in Fig. 7). However, the preferential enrichment of garnet in Fe displaces the reaction to lower pressures. Similarly, the reaction Opx + Spl + Crn = Spr, limiting the stability field of the assemblage pyroxene–spinel–corundum from reaction domains A2, should be displaced to higher temperatures with increasing Fe content in spinel.

Obviously, the *P–T* evolution of reaction domains A (Px–Spl–Crn–Crt) is identical to that of domains B (Spl–Spr–Sil–Grt), and the metamorphic assemblages from both domains correspond to the same *P–T* path. The large mismatch in relative pressures and temperatures characterizing the metamorphic evolution of both domains in the MAS and CMAS petrogenetic grids shown in Fig. 7 is, therefore, not realistic and should disappear under the influence of additional chemical components [see figs 9 and 12 of Kelly & Harley (2004), also illustrating the sensitivity of the simplified MAS and CMAS reactions to additional components]. The overall *P–T* path of the Mg–Al granulites cannot be quantified but should be characterized by cooling, accompanied or followed by some compression.

METAMORPHIC REACTIONS IN THE Ca–Al HIBONITE-BEARING GRANULITES

The Ca–Al granulites correspond to troctolitic protoliths, with the normative abundances of olivine and plagioclase ranging from 95·3 to 98·7%. Compared with the Mg–Al sapphirine-bearing granulites, they are less magnesian and more rich in Ca, Al and alkalis. They contain quartz and are relatively rich in clinopyroxene, whereas orthopyroxene is absent. Xenoliths 1904-1 and 1904-9 contain hibonite that is probably a magmatic relict (see the section on 'Pre-metamorphic vs metamorphic mineral assemblages'), whereas all other minerals, possibly with the exception of some spinel, were formed by subsolidus reactions. The major metamorphic features to be explained include:

(1) the mineral assemblage formed by the initial subsolidus reactions;
(2) the assemblage Qtz Cpx I;
(3) the spinel I–sillimanite–garnet corona textures;
(4) the close association of corundum and Cpx II;
(5) the development of garnet at the expense of plagioclase and corundum;
(6) the association Spl II + Crn enriched in Cr.

(1) Similarly to the Mg–Al granulites, the initial metamorphic mineral assemblage of the Ca–Al granulites may have been represented by pyroxenes, spinel and plagioclase formed at the expense of the igneous troctolitic assemblage olivine + plagioclase.

(2) The assemblage Qtz + Cpx I does not include any additional minerals. As plagioclase seems to have been stable throughout the entire evolution, a plausible explanation for this assemblage invokes the reaction Ab + Cpx = Qtz + Jd–Cpx. This continuous reaction, first studied by Kushiro (1969) and subsequently considered by a number of researchers (see Anovitz, 1991, and references therein), has a positive *P–T* slope. Its isopleth for 20% of jadeite in clinopyroxene is shown in Fig. 7 relative to the CMAS simplified petrogenetic grid. Clinopyroxene I accommodates 14–19% jadeite and could, thus, have formed from plagioclase and a less Na-rich clinopyroxene by cooling and/or compression. At this stage, spinel from the initial metamorphic mineral assemblage (1) may have still been stable. Hibonite, of which the equilibrium assemblage with quartz is unknown in nature, may have been partially replaced by mullite and sillimanite.

(3) As temperature decreases and/or pressure increases, clinopyroxene I tends to accommodate more jadeite, until the competitive reaction Spl + Qtz = Sil + Grt is realized. The combined reaction Spl + Pl + Cpx I = Sil + Grt + Cpx II replaces Ab + Cpx = Qtz + Jd–Cpx. It is inferred to be responsible for both the sillimanite–garnet coronas after spinel I (Fig. 5c) and clinopyroxene II forming independent grains and mantling the Cpx I–Qtz cores (Figs 2c and 5a). Similar mineral relations, although rather unusual for granulites in general, are known from granulite-facies rocks of the Parautochtonous Belt, Grenville (Indares & Rivers, 1995).

(4) The assemblage Crn + Cpx II (Fig. 2c) is consistent with the reaction Spl + Pl = Crn + Cpx, as observed in the Mg–Al granulite xenoliths (see the previous section and Fig. 7). As corundum is unstable with quartz over a vast range of metamorphic conditions (e.g. Shulters & Bohlen, 1989), this assemblage must be considered to have formed late with respect to quartz, when the latter had already been isolated in the core parts of the complexly built grains of clinopyroxene I–II. The lack of orthopyroxene in this assemblage is probably due to temperatures too high to stabilize the assemblages Opx + Crn and Opx + Crn + Spl (see Fig. 7).

(5) The 'flaky' and massive zones of garnet or garnet and clinopyroxene propagating and resorbing plagioclase (Fig. 2c and 5a) are inferred to have formed from the reactions Di–Cpx + Spl + Pl = Grt and Di–Cpx + Spl + Pl = Grt + Tsch-rich Cpx analogous to the reactions Cpx + Opx + Spl + Pl = Grt and Opx + Spl + Pl = Grt + Cpx in the Mg–Al granulites. Petrographically, garnet developed at the expense of corundum (Figs 2c and 5f) can definitely be attributed to the reactions Cpx + Crn = Grt, as well as the resorption by garnet of those pyroxene grains that are located close to corundum. Similarly to the reaction Opx + Crn = Grt, this garnet-forming reaction is characterized by a negative dP/dT slope (Gasparik, 1984*b*) and may become operative during the course of metamorphic compression.

(6) The association Spl II + Crn can be explained by the reaction Crn + Grt = Spl + Sil, again in good agreement with the petrography (Fig. 5f). Unusually high Cr contents in spinel II seem to stabilize the assemblage Spl + Sil at relatively high pressures and low temperatures that are inconsistent with its stability field in Cr-free system (e.g. Shulters & Bohlen, 1989).

In summary, the reaction textures observed in the Ca–Al granulites are consistent with cooling accompanied or followed by compression during the formation of garnet at the expense of corundum and clinopyroxene.

MINERAL ZONING AS AN INDICATOR OF METAMORPHIC EVOLUTION

In the Mg–Al sapphirine-bearing granulites, considerable chemical zonation is found in pyroxenes only (Fig. 4a–f). Opx I shows a rimwards decrease in Al, Ca and Na (Fig. 4a). Because the reaction Ol + Pl = Opx + Cpx + + Spl ± Crn takes place at relatively high temperature, Opx I should equilibrate with clinopyroxene, spinel and plagioclase. The Al content in Opx equilibrated with Spl and Pl is controlled by both pressure and temperature (Gasparik, 1984*a*; Berchova, 1996), whereas the Ca and Na contents in the case of equilibration with clinopyroxene are controlled chiefly by temperature (Brey & Köhler, 1990; Berchova, 1996). The concentrations of these elements decrease with a decrease in temperature. Thus, we suggest that cooling is mainly responsible for the observed chemical zonation in Opx I. Opx II is either nearly homogeneous (sp. 1904-3; Fig. 4b) or shows different patterns in the same textural context, indicating poor equilibration (sp. 1904-7; Fig. 4c and d).

Cpx II in the Mg–Al sapphirine-bearing granulites shows either a rimwards increase in the Al content (sp. 1904-3; Fig. 4e) or varying zoning patterns indicative of poor equilibration (sp. 1904-7; Fig. 4f). The largest grains of Cpx II are always characterized by plateaux in the core. It is, therefore, inferred that these grains record early metamorphic stabilization possibly corresponding to the reaction Ol + Pl = Cpx + Opx + Spl ± Crn during post-magmatic cooling/compression. Their further history involves the diopside and enstatite-consuming reactions Pl + Cpx + Opx + Spl = Grt and Cpx + Opx + Crn = Grt that cause the observed enrichment in Al and Na (Fig. 4e and f).

In the Ca–Al hibonite-bearing granulites, only Cpx II and Crn associated with Spl II show considerable zoning. In Cpx II, all available profiles are characterized by a rimwards increase in Al content that, however, tends to decrease again within the 20 μm outermost rim (Fig. 6a–e). Normally, the largest Cpx II grains have an Al plateau in the core (Fig. 6a and b). They are interpreted to record the reaction Spl + Ab + Cpx I = Sil + Grt + Cpx II in the course of early cooling and/or compression. Their subsequent history, similarly to clinopyroxene from the Mg–Al granulites, involves the reactions Pl + Cpx + Spl = Grt and Cpx + Crn = Grt that consume the diopside component in clinopyroxene and cause its enrichment in the Tschermak and jadeite components (Fig. 6a–e).

In both Mg–Al and Ca–Al granulites, the Mg-number in clinopyroxene increases rimwards. This is consistent with cooling in the presence of garnet, when clinopyroxene preferentially accommodates Mg, while garnet takes up Fe^{2+} (e.g. Ai, 1994; Krogh Ravna, 2000). In both rock types, the reaction Di + Ab + Spl = Sil + Grt + Jd–Di appears to have progressed in the reverse direction at the very end of the reaction path. More diopside-rich clinopyroxene (Al and Na decrease at the outermost rims of Cpx II in Fig. 6a–e), Na-rich plagioclase (thin Pl mantles around clinopyroxene) and 'secondary' spinel (thin rims of Spl II mantling sillimanite in the Spl–Sil–Grt corona textures) were formed. These indications of late retrogression are minor.

DISCUSSION

P–T path of the granulites and its geodynamic significance

The geothermometric estimates for the Mg–Al sapphirine-bearing granulites suggest cooling from near-solidus temperatures of at least 1090–1135°C to 514–784°C. The metamorphic reaction path is consistent with cooling associated with or followed by compression, the latter resulting in the development of garnet at the expense of mafic minerals, plagioclase and corundum. The sequence of reactions observed in the Ca–Al hibonite-bearing granulites is also consistent with subsolidus cooling to ~640–740°C and compression.

The observed reaction sequence and available *P–T* estimates do not allow us to evaluate the *P–T* trend of the studied granulites at the end of their *P–T* path, as no

convincing petrographic evidence on their retrograde evolution exists. In contrast to exposed granulites where both clockwise and anticlockwise anticlockwise P–T paths are often characterized by pronounced decompression in the course of tectonic exhumation, no indications of this stage are found in our samples. The lack of hydrous minerals also argues against considerable retrogression.

Nevertheless, the inferred reaction sequence leading to the formation of sapphirine–sillimanite–garnet coronas on spinel (reaction domain B) and aggregates of Tschermak-rich clinopyroxene and sillimanite (reaction domain D) in the Mg–Al granulites may hint at an anticlockwise P–T evolution (see the section on 'Metamorphic reactions' and Fig. 7). This mode of evolution accords with the detailed results of Appel *et al.* (1998) and Möller *et al.* (1998) on the Pan-African granulite terranes of eastern and northeastern Tanzania (Pare, Usambara and Uluguru mountains) situated south and SW of the Chyulu Hills (Fig. 1). For metasedimentary and meta-igneous granulites from these localities, Appel *et al.* (1998) proposed an anticlockwise P–T path with the peak conditions of approximately 810°C and 9·5–11 kbar. As the cause of the granulite metamorphism, those workers and Möller *et al.* (2000) put forward a model of magmatic underplating in the environment of juvenile arc terranes forming the Mozambique belt in Pan-African times.

This model is in good agreement with the fact that the studied samples represent a former igneous suite. The inferred metamorphic reaction path associated with compression also accords with the geochemical and petrographic characteristics of websterite xenoliths from the studied cumulate sequence. The geochemical features of the websterites, such as positive Eu anomalies and elevated Ni abundances, suggest plagioclase- and olivine-rich gabbroic protoliths and thus shallow-level plagioclase accumulation. At the same time, their actual mineral assemblages (pyroxenes, spinel, garnet and olivine) correspond to upper mantle pressures and temperatures (18–22 kbar and 927–1007°C for most specimens; Ulianov *et al.*, in preparation). To reconcile this apparent contradiction, Ulianov *et al.* (in preparation) favour a model of compression by foundering of dense lower crustal material into the mantle, probably towards the end of Pan-African subduction and accretion. Such a process is possible in areas with high geothermal gradients such as magmatic arcs (Jull & Kelemen, 2001) and is observed today in the southern Sierra Nevada (Ducea, 2001; Boyd *et al.*, 2004; Zandt *et al.*, 2004).

Mineral assemblages and their petrogenetic significance

Meta-igneous granulites rich in Mg, Al and Ca, such as the xenoliths from this study, are rare. Of all the xenolith localities studied, the P–T path responsible for the observed mineralogy has been specified only for Kerguelen (Grégoire *et al.*, 1998). For the Stockdale and Delegate granulites, the reaction sequences and possible P–T paths were reviewed by Christy (1989) on the basis of a CMAS petrogenetic grid developed for the assemblage Cpx + Opx + Pl + Spr + Sil + Grt. All these paths are largely characterized by cooling. In contrast, the mafic sapphirine-bearing granulites from metamorphic terranes, with the exception of Finero (Christy, 1989), demonstrate decompression-dominated reaction sequences and P–T paths, in which sapphirine occurs in symplectitic intergrowths with plagioclase found after kyanite (Johansson & Möller, 1986; Carswell *et al.*, 1989; Christy, 1989; Grant, 1989; Möller, 1999).

The Mg–Al sapphirine-bearing granulite xenoliths have similarities to the granulite xenoliths from the Stockdale kimberlite in Kansas (Meyer & Brookins, 1976). Except for the lack of corundum, their phase assemblage is the same and there are clear similarities in mineral chemistry. The Spl–Spr–Sil–Grt corona textures described from Stockdale are similar to those described in this study and were interpreted as indicating a cooling-dominated metamorphic path (Christy, 1989).

The Ca–Al hibonite-bearing granulites are unique, because of the geochemical characteristics and unusual mode of formation of hibonite and because of the uncommon metamorphic reaction sequence observed in the host rocks. The studied hibonite is very poor in La, Ce, Th and Y. These low abundances are rather uncommon for terrestrial hibonites, as the latter, except for one locality (Punalur, India), are enriched in LREE and Th (Maaskant *et al.*, 1980; Santosh *et al.*, 1991; Rakotondrazafy *et al.*, 1996). Low concentrations of La, Ce, Th and Y are typical, however, for hibonite from meteorites (e.g. Fahey *et al.*, 1987). Si is higher than in any other terrestrial hibonite. All known terrestrial (Yakovlevskaya, 1961; Maaskant *et al.*, 1980; Sandiford & Santosh, 1991; Rakotondrazafy *et al.*, 1996) and extraterrestrial occurrences (e.g. Fahey *et al.*, 1987) represent strongly silica-undersaturated lithologies. In the samples from this study, however, the rocks are not highly depleted in silica, resulting in modal quartz formed in the course of metamorphism. Thus, strong Si undersaturation is not universal for hibonite-bearing rocks. In all known terrestrial occurrences, hibonite is considered as a metamorphic (possibly metasomatic) mineral. In the samples studied here, it seems to represent a magmatic relict (see the section on 'Pre-metamorphic vs metamorphic mineral assemblages'). The mullite in the studied samples represents the first occurrence reported of 2:1 mullite in nature. Synthetic mullite of such composition is common (e.g. Angel & Prewitt, 1986; Angel *et al.*, 1991). Mullite from natural occurrences is, however,

always more Si-rich, i.e. intermediate between the 3:2 and 2:1 types (Deer *et al.*, 1982; Preston *et al.*, 1999).

The early reaction sequence inferred from these granulites is rather uncommon. It is essentially based on the equilibria Ab + Cpx = Qtz + Jd–Cpx and Spl I + Qtz = Sil + Grt. Quartz seems arrested in the cores of clinopyroxene I and is not equilibrated with garnet; corundum forms instead. Thus, despite being formally 'orthopyroxene-free garnet + clinopyroxene + quartz metabasites' these rocks deviate from the paragenetic definition and reaction model (based on the prograde equilibria Opx + Pl = Grt + Cpx + Qtz) for common representatives of this rock family (see O'Brien & Rötzler, 2003; Pattison, 2003).

In a more general sense, it is worth emphasizing that the studied granulites preserve high-temperature textures (especially the Spl–Cpx–Opx symplectitic intergrowth in the Mg–Al sapphirine-bearing granulites and Qtz–Cpx I intergrowth in the Ca–Al hibonite-bearing granulites). At the same time, they show (almost) no petrographic evidence of lower-T retrograde evolution.

SUMMARY AND CONCLUSIONS

Together with spinel–garnet websterites entrained from the lithospheric mantle, the Mg–Al sapphirine-bearing and Ca–Al hibonite-bearing granulites from the Chyulu Hills volcanic field, Kenya, represent a former igneous suite of gabbroic to troctolitic cumulates. All olivine has been removed by subsolidus reactions and plagioclase was texturally and compositionally modified in the course of metamorphism. Relicts of the igneous stage in the Mg–Al granulites may include calcium-rich orthopyroxene and some spinel. Geothermometric calculations based on the Ca contents in early orthopyroxene give a minimum temperature estimate of 1090–1135°C. In the Ca–Al granulites, hibonite and possibly some spinel are texturally the oldest minerals in the crystallization sequence; these are possibly igneous relicts.

The igneous minerals have, to a large degree, been replaced by metamorphic mineral assemblages. Geothermobarometric estimates for metamorphic parageneses indicate cooling from (near) igneous temperatures to conditions of ~600–740°C. The observed reaction sequence is consistent with cooling accompanied or followed by compression. The distinctive reaction textures include Cpx–Opx–Spl (± Crn) intergrowths replacing igneous olivine and plagioclase and Crn–Cpx symplectites after spinel and plagioclase in the Mg–Al granulites, quartz–diopside intergrowths formed at the expense of early plagioclase and clinopyroxene in the Ca–Al granulites, as well as the prominent corona textures observed in both rock types. All of these textures seem to have been acquired at granulite-facies conditions.

In a more general context, the studied granulite xenoliths have few direct analogues in both xenolith suites and granulite terranes. The Mg–Al granulites are most comparable with granulite xenoliths from the Stockdale kimberlite in Kansas (Meyer & Brookins, 1976). The Ca–Al hibonite-bearing granulites are unique with respect to textures, whole-rock composition, and the compositions of hibonite and mullite. Both rock types enlarge the spectrum of known Ca–Al–Mg-rich granulites and contribute to the general understanding of reaction sequences in the CMAS system at granulite-facies conditions.

ACKNOWLEDGEMENTS

Hans-Peter Meyer and Edwin Gnos are thanked for assistance with electron microprobe analysis. Rainer Altherr is thanked for discussion and critical comments on the manuscript. We are grateful to Simon Harley and Tomoaki Morishita for their detailed and constructive reviews, which helped us to significantly improve the earlier version of this paper, and Marjorie Wilson for her valuable comments and editorial handling of the manuscript. Permission and help for field sampling provided by the Office of the President, Kenya Wildlife Service, and the Kenya Agricultural Research Institute in Kiboko are gratefully acknowledged. Field work was financially supported by the Deutsche Forschungsgemeinschaft within the frame of the Collaborative Research Center 108 (SFB 108) at the University of Karlsruhe. The research was supported by the Swiss National Science Foundation grant 200021-100647/1.

REFERENCES

Ai, Y. (1994). A revision of the garnet–clinopyroxene Fe^{2+}–Mg exchange geothermometer. *Contributions to Mineralogy and Petrology* **115**, 467–473.

Angel, R. J. & Prewitt, C. T. (1986). Crystal structure of mullite: a reexamination of the average structure. *American Mineralogist* **71**, 1472–1482.

Angel, R. J., McMullan, R. K. & Prewitt, C. T. (1991). Substructure and superstructure of mullite by neutron diffraction. *American Mineralogist* **76**, 332–342.

Anovitz, L. M. (1991). Al zoning in pyroxene and plagioclase: window on late prograde to early retrograde P–T path in granulite terranes. *American Mineralogist* **76**, 1328–1343.

Appel, P. (1996). Hochdruckgranulite und Eklogite im Mozambique Belt von Tanzania: eine petrologische und geochemische Studie. PhD Thesis, Christian-Albrechts-Universität Kiel.

Appel, P., Möller, A. & Schenk, V. (1998). High-pressure granulite facies metamorphism in the Pan-African belt of eastern Tanzania: P–T–t evidence against granulite formation by continent collision. *Journal of Metamorphic Geology* **16**, 491–509.

Attoh, K. (1998). Models for orthopyroxene–plagioclase and other corona reactions in metanorites, Dahomeyide orogen, West Africa. *Journal of Metamorphic Geology* **16**, 345–362.

Baker, B. H., Williams, L. A. J., Miller, J. A. & Fitch, F. J. (1971). Sequence and geochronology of the Kenya rift volcanics. *Tectonophysics* **11**, 191–215.

Beckett, J. R. & Stolper, E. (1994). The stability of hibonite, melilite and other aluminous phases in silicate melts: implications for the origin of hibonite-bearing inclusions from carbonaceous chondrites. *Meteoritics*, **29**, 41–65.

Bell, K. & Dodson, M. H. (1981). The geochronology of the Tanzanian Shield. *Journal of Geology* **89**, 109–128.

Berchova, V. (1996). Experimentelle Orthopyroxen-Klinopyroxen Thermobarometric in CaO–MgO–Al_2O_3–SiO_2–H_2O (CMASH) System. PhD Thesis. Ludwig-Maximilians-Universität, München, Germany.

Bhattacharya, S. & Kar, R. (2002). High-temperature dehydration melting and decompressive *P–T* path in a granulite complex from the Eastern Ghats, India. *Contributions to Mineralogy and Petrology* **143**, 175–191.

Bohlen, S. R. (1987). Pressure–temperature–time path and a tectonic model for the evolution of granulites. *Journal of Geology* **95**, 617–632.

Bohlen, S. R. (1991). On the formation of granulites. *Journal of Metamorphic Geology* **9**, 223–229.

Bohlen, S. R., Dollase, W. A. & Wall, V. J. (1986). Calibration and applications of spinel equilibria in the system FeO–Al_2O_3–SiO_2. *Journal of Petrology* **27**, 1143–1156.

Boyd, O. S., Craig, H. J. & Sheehan, A. F. (2004). Foundering lithosphere imaged beneath the southern Sierra Nevada. *Science* **305**, 660–662.

Brey, G. P. & Köhler, T. (1990). Geothermobarometry in four-phase lherzolites II. New thermobarometers, and practical assessment of existing thermobarometers. *Journal of Petrology* **31**, 1353–1378.

Cahen, L., Snelling, N. J., Delhal, J. & Vail, J. R. (1984*)*. *The Geochronology and Evolution of Africa*. Oxford: Clarendon Press, 512 pp.

Cameron, W. E. (1977). Mullite: a substituted alumina. *American Mineralogist* **62**, 747–755.

Carswell, D. A. (1975). Primary and secondary phlogopites in garnet lherzolite xenoliths. *Physics and Chemistry of the Earth* **9**, 417–430.

Carswell, D. A., Möller, C. & O'Brien, P. J. (1989). Origin of sapphirine–plagioclase symplectites in metabasites from Mitterbachgraben, Dunkelsteinerwald granulite complex, Lower Austria. *European Journal of Mineralogy* **1**, 455–466.

Christy, A. G. (1989). The stability of sapphirine + clinopyroxene: implications for phase relations in the CaO–MgO–Al_2O_3–SiO_2 system under deep-crustal and upper mantle conditions. *Contributions to Mineralogy and Petrology* **102**, 422–428.

Coolen, J. J. M. M. M., Priem, H. N. A., Verdurmen, E. A. T. & Verschure, R. H. (1982). Possible zircon U–Pb evidence for Pan-African granulite-facies metamorphism in the Mozambique Belt of southern Tanzania. *Precambrian Research* **17**, 31–40.

Dawson, J. B. (1977). Sub-cratonic crust and upper mantle models based on xenolith suites in kimberlite and nephelinitic diatremes. *Journal of the Geological Society, London* **134**, 173–184.

Dawson, J. B., Harley, S. L., Rudnick, R. L. & Ireland, T. R. (1997). Equilibration and reaction in Archaean quartz–sapphirine granulite xenoliths from the Lace kimberlite pipe, South Africa. *Precambrian Research* **104**, 123–146.

Deer, W. A., Howie, R. A. & Zussman, J. (1982). *Rock-forming Minerals. Volume 1A: Orthosilicates*. Harlow: Longman, pp. 742–758.

Downes, H. (1993). The nature of the lower continental crust of Europe: petrological and geochemical evidence from xenoliths. *Physics of the Earth and Planetary Interiors* **79**, 195–218.

Downes, H., Dupuy, C. & Leyreloup, A. F. (1990). Crustal evolution of the Hercynian belt of western Europe: evidence from lower-crustal granulitic xenoliths (French Massif Central). *Chemical Geology* **83**, 209–231.

Drake, M. J. & Boynton, W. L. (1988). Partitioning of rare earth elements between hibonite and melt and implications for nebular condensation of the rare earth elements. *Meteoritics* **23**, 75–80.

Ducea, M. N. (2001). The California arc: thick granitic batholiths, eclogitic residues, lithospheric-scale thrusting, and magmatic flare-ups. *GSA Today* **11**, 4–10.

Evans, R. J., Ashwal, L. D. & Hamilton, M. A. (1999). Mafic, ultramafic, and anorthositic rocks of the Tete Complex, Mozambique: petrology, age, and significance. *South African Journal of Geology* **102**, 153–166.

Fahey, A. J., Goswani, J. N., McKeegan, K. D. & Zinner, E. (1987). ^{26}Al, ^{244}Pu, ^{50}Ti, REE and trace element abundances in hibonite grains from CM and CV meteorites. *Geochimica et Cosmochimica Acta* **51**, 329–350.

Gasparik, T. (1984*a*). Two-pyroxene thermobarometry with new experimental data in the system CaO–MgO–Al_2O_3–SiO_2. *Contributions to Mineralogy and Petrology* **87**, 87–97.

Gasparik, T. (1984*b*). Experimental determined stability of clinopyroxene + garnet + corundum in the system CaO–MgO–Al_2O_3–SiO_2. *American Mineralogist* **69**, 1025–1035.

Gasparik, T. (2003). *Phase Diagrams for Geoscientists: an Atlas of the Earth's Interior*. Berlin: Springer, 462 pp.

Gichile, S. (1992). Granulites in the Precambrian basement of southern Ethiopia: geochemistry, *P–T* conditions of metamorphism and tectonic setting. *Journal of African Earth Sciences* **15**, 251–263.

Grant, S. M. (1989). Tectonic implications from sapphirine-bearing lithologies, south-west Grenville Province, Canada. *Journal of Metamorphic Geology* **7**, 583–598.

Green, D. H. & Ringwood, A. E. (1967). An experimental investigation of the gabbro to eclogite transformation and its petrologic application. *Geochimica et Cosmochimica Acta* **3**, 767–834.

Grégoire, M., Cottin, J. Y., Giret, A., Mattielli, N. & Weis, D. (1998). The meta-igneous granulite xenoliths from Kerguelen Archipelago: evidence of a continent nucleation in an oceanic setting. *Contributions to Mineralogy and Petrology* **133**, 259–283.

Griffin, W. L. (1971). Genesis of coronas in anorthosites of the Upper Jotun Nappe, Indre Song, Norway. *Journal of Petrology* **12**, 219–243.

Griffin, W. L. & O'Reilly, S. Y. (1986). Mantle-derived sapphirine. *Mineralogical Magazine* **50**, 635–640.

Harley, S. L. (1984). An experimental study of the partitioning of Fe and Mg between garnet and orthopyroxene. *Contributions to Mineralogy and Petrology* **86**, 359–373.

Harley, S. L. (1989). The origin of granulites: a metamorphic perspective. *Geological Magazine* **126**(3), 215–247.

Haug, G. H. & Strecker, M. R. (1995). Volcano-tectonic evolution of the Chyulu Hills and implication for the regional stress field in Kenya. *Geology* **23**, 165–168.

Henjes-Kunst, F. & Altherr, R. (1992). Metamorphic petrology of xenoliths from Kenya and Northern Tanzania and implications for geotherms and lithospheric structure. *Journal of Petrology* **33**, 1125–1156.

Herzberg, C. T. (1978). Pyroxene geothermometry and geobarometry: experimental and thermodynamic evaluation of some subsolidus phase relations involving pyroxenes in the system CaO–MgO–Al_2O_3–SiO_2. *Geochimica et Cosmochimica Acta* **42**, 945–957.

Holmes, A. (1951). The sequence of Precambrian orogenic belts in south and central Africa. In: *Proceedings of the 18th International Geological Congress, Part XXIV*. London: Geological Society, pp. 254–269.

Huang, Y.-M., Van Calsteren, P. & Hawkesworth, C. J. (1995). The evolution of the lithosphere in southern Africa: a perspective on the basic granulite xenoliths from kimberlites in South Africa. *Geochimica et Cosmochimica Acta* **59**, 4905–4920.

Indares, A. D. (2003). Metamorphic textures and *P–T* evolution of high-*P* granulites from the Lelukuau terrane, NE Grenville Province. *Journal of Metamorphic Geology* **21**, 35–48.

Indares, A. D. & Rivers, T. (1995). Textures, metamorphic reactions and thermobarometry of eclogitized metagabbros: a Proterozoic example. *European Journal of Mineralogy* **7**, 43–56.

Irving, A. J. (1974). Geochemical and high pressure experimental studies of garnet pyroxenite and pyroxene granulite xenoliths from the Delegate basaltic pipes, Australia. *Journal of Petrology* **15**, 1–40.

Jan, M. Q. & Howie, R. A. (1981). The mineralogy and geochemistry of the metamorphosed basic and ultrabasic rocks of the Jijal complex, Kohistan, NW Pakistan. *Journal of Petrology* **22**, 85–126.

Johansson, L. & Möller C. (1986). Formation of sapphirine during retrogression of a basic high-pressure granulite, Roan, Western Gneiss Region, Norway. *Contributions to Mineralogy and Petrology* **94**, 29–41.

Jones, A. P., Smith, J. V., Hansen, E. C. & Dawson, J. B. (1983). Metamorphism, partial melting and K-metasomatism of garnet–scapolite–kyanite granulite xenoliths from Lashaine, Tanzania. *Journal of Geology* **91**, 143–165.

Jull, M. & Kelemen, P. B. (2001) On the conditions of lower crustal convective instability. *Journal of Geophysical Research* **106**, 6423–6446.

Kebede, T., Kloetzli, U. S. & Koeberl, C. (2001). U/Pb and Pb/Pb zircon ages from granitoid rocks of Wallagga area: constraints on magmatic and tectonic evolution of Precambrian rocks of western Ethiopia. *Mineralogy and Petrology* **71**, 251–271.

Keil, K. & Fuchs, L. H. (1971) Hibonite ($Ca_2(Al,Ti)_{24}O_{38}$) from the Leoville and Allende chondritic meteorites. *Earth and Planetary Science Letters* **12**, 184–190.

Kelly, N. M. & Harley, S. L. (2004) Orthopyroxene–corundum in Mg–Al-rich granulites from the Oygarden Islands, East Antarctica. *Journal of Petrology* **45**, 1481–1512.

Kempton, P. D., Harmon, R. S., Hawkesworth, C. J. & Moorbath, S. (1990). Petrology and geochemistry of lower crustal granulites from the Geronimo Volcanic Field, southern Arizona. *Geochimica et Cosmochimica Acta* **54**, 3401–3426.

Kempton, P. D., Downes, H., Neymark, L. A., Wartho, J. A., Zartman, R. E. & Sharkov, E. V. (2001). Garnet granulite xenoliths from the Northern Baltic Shield—the underplated lower crust of a Palaeoproterozoic large igneous province? *Journal of Petrology* **42**, 731–763.

Kennedy, A. K., Lofgren, G. E. & Wasserburg, G. J. (1994). Trace-element partition coefficients for perovskite and hibonite in meteorite compositions. *Chemical Geology* **117**, 379–390.

Key, R. M., Charsley, T. J., Hackman, B. D., Wilkinson, A. F. & Rundle, C. C. (1989). Superimposed Upper Proterozoic collision-controlled orogenies in the Mozambique Orogenic Belt of Kenya. *Precambrian Research* **44**, 197–225.

Kretz, R. (1983). Symbols for rock-forming minerals. *American Mineralogist* **68**, 277–279.

Kriegsman, L. M. & Schumacher, J. C. (1999). Petrology of sapphirine-bearing and associated granulites from central Sri Lanka. *Journal of Petrology* **40**, 1211–1239.

Krogh Ravna, E. (2000). The garnet–clinopyroxene Fe–Mg geothermometer: an updated calibration. *Journal of Metamorphic Geology* **18**, 211–219.

Kröner, A., Greiling, R., Reischmann, T., Hussein, I. M., Stern, R. J., Dürr, S., Krüger J. & Zimmer, M. (1987). Pan-African crustal evolution in the Nubian segment of northeast Africa. In: Kröner, A. (ed.) *Proterozoic Lithospheric Evolution. American Geophysical Union, Washington, DC, Geodynamic Series* **17**, 235–257.

Kröner, A., Muhongo, S., Hegner, E. & Wingate, M. T. D. (2003). Single zircon geochronology and Nd isotopic systematics of Proterozoic high-grade rocks from the Mozambique belt of southern Tanzania (Masasi area): implications for Gondwana assembly. *Journal of the Geological Society, London* **160**, 745–758.

Kushiro, I. (1969). Clinopyroxene solid solutions formed by reaction between diopside and plagioclase at high pressures. *Mineralogical Society of America, Special Paper* **2**, 179–191.

Kushiro, I. & Yoder, H. S. (1966). Anorthite–forsterite and anorthite–enstatite reactions, and their bearing on the basalt–eclogite transformation. *Journal of Petrology* **7**, 337–362.

Lensch, G. (1971). Das Vorkommen von Sapphirin im Peridotitkörper von Finero (Zone von Ivrea, Italienische Westalpen). *Contributions to Mineralogy and Petrology* **31**, 145–153.

Lui, I. C. & Presnall, D. C. (1990). Liquidus phase relations in the join anorthite–forsterite–quartz at 20 kbar with applications to basalt petrogenesis and igneous sapphirine. *Contributions to Mineralogy and Petrology* **104**, 735–742.

Liu, I. C. & Presnall, D. C. (2000). Liquidus phase relations in the system $CaO–MgO–Al_2O_3–SiO_2$ at 2·0 GPa: applications to basalt fractionation, eclogites and igneous sapphirine. *Journal of Petrology* **41**, 3–20.

Maaskant, P., Coolen, J. J. M. & Burke, E. A. J. (1980). Hibonite and coexisting zoisite and clinozoisite in a calc-silicate granulite from southern Tanzania. *Mineralogical Magazine* **43**, 995–1003.

MacDougall, J. D. (1979). Refractory-element-rich inclusions in CM meteorites. *Earth and Planetary Science Letters* **42**, 1–6.

Meert, J. G. (2003). A synopsis of events related to the assembly of eastern Gondwana. *Tectonophysics*, **362**, 1–40.

Meyer, H. O. A. & Brookins, D. G. (1976). Sapphirine, sillimanite and garnet in granulite xenoliths from Stockdale kimberlite, Kansas. *American Mineralogist* **61**, 1194–1202.

Möller, A., Appel, P., Mezger, K. & Schenk, V. (1995). Evidence for a 2 Ga subduction zone: eclogites in the Usaragan Belt of Tanzania. *Geology* **23**, 1067–1070.

Möller, A., Mezger, K. & Schenk, V. (1998). Crustal age domains and the evolution of the continental crust in the Mozambique Belt of Tanzania: combined Sm–Nd, Rb–Sr and Pb–Pb isotopic evidence. *Journal of Petrology* **39**, 749–783.

Möller, A., Mezger, K. & Schenk, V. (2000). U–Pb dating of metamorphic minerals: Pan-African metamorphism and prolonged slow cooling of high pressure granulites in Tanzania, East Africa. *Precambrian Research* **104**, 123–146.

Möller, C. (1999). Sapphirine in SW Sweden: a record of Sveconorwegian (-Grenvillian) late-orogenic tectonic exhumation. *Journal of Metamorphic Geology* **17**, 121–141.

Montanini, A. & Tribuzio, R. (2001). Gabbro-derived granulites from the northern Apennines (Italy): evidence for lower-crustal emplacement of tholeiitic liquids in post-Variscan times. *Journal of Petrology* **42**, 2259–2277.

Morishita, T. & Arai, S. (2001). Petrogenesis of corundum-bearing mafic rocks in the Horoman Peridotite complex, Japan. *Journal of Petrology* **42**, 1279–1299.

Muhongo, S. M. & Lenoir, J.-L. (1994). Pan-African granulite-facies metamorphism in the Mozambique belt of Tanzania: U–Pb zircon geochronology. *Journal of the Geological Society, London* **151**, 343–347.

Muhongo, S. M., Kröner, A. & Nemchin, A. A. (2001). Zircon ages from granulite facies rocks in the Mozambique belt of Tanzania and implications for Gondwana assembly. *Journal of Geology* **109**, 171–189.

Müntener, O., Hermann, J. & Trommsdorff, V. (2000). Cooling history and exhumation of lower crustal granulites and upper

mantle (Malenco, Eastern Central Alps). *Journal of Petrology* **41**, 175–200.

Nichols, G. T., Berry, R. F. & Green, D. H. (1992). Internally consistent gahnitic spinel–cordierite–garnet equilibria in the FMASHZn system: geothermobarometry and applications. *Contributions to Mineralogy and Petrology* **111**, 362–377.

Novak, O., Ritter, J. R. R., Altherr, R., Garasic, V., Volker, F., Kluge, C., Kaspar, T., Byrne, G. F., Sobolev, S. V. & Fuchs, K. (1997). An integrated model for the deep structure of the Chyulu Hills volcanic field, Kenya. *Tectonophysics* **278**, 187–209.

O'Brien, P. J. & Rötzler, J. (2003). High-pressure granulites: formation, recovery of peak conditions and implications for tectonics. *Journal of Metamorphic Geology* **21**, 3–20.

Omenge, J. M. & Okelo, R. E. (1992). *Geology of the Chyulu–Oloitokitok area*. Kenya Mines and Geology Department, Nairobi, Report 112, 51 pp.

Osanai, Y., Hammamoto, T., Maishima, O. & Kagami, H. (1998). Sapphirine-bearing granulites and related high-temperature metamorphic rocks from the Higo metamorphic terrane, west central Kyushu, Japan. *Journal of Metamorphic Geology* **16**, 53–66.

Ouzegane, K., Guiraud, M. & Kienast, J. R. (2003). Prograde and retrograde evolution in high-temperature corundum granulites (FMAS and KFMASH systems) from In Ouzzal Terrane (NW Hoggar, Algeria). *Journal of Petrology* **44**, 517–545.

Pattison, D. R. M. (2003). Petrogenetic significance of orthopyroxene-free garnet + clinopyroxene + plagioclase ± quartz-bearing metabasites with respect to the amphibolite and granulite facies. *Journal of Metamorphic Geology* **21**, 21–34.

Pinna, P., Jourde, G., Calvez, J. Y. & Mroz, J. P. (1993). The Mozambique Belt in northern Mozambique: Neoproterozoic (1100–850 Ma) crustal growth and tectogenesis, and superimposed Pan-African (800–550 Ma) tectonism. *Precambrian Research* **62**, 1–59.

Preston, J. P., Dempster, T. J., Bell, B. R. & Rogers, G. (1999). The petrology of mullite-bearing peraluminous xenoliths: implications for contamination processes in basaltic magmas. *Journal of Petrology* **40**, 549–573.

Rakotondrazafy, M. A. F., Moine, B. & Cuney, M. (1996). Mode of formation of hibonite ($CaAl_{12}O_{19}$) within the U–Th skarns from the granulites of SE Madagascar. *Contributions to Mineralogy and Petrology* **123**, 190–201.

Rickers, K, Raith, M. & Dasgupta, S. (2001). Multistage reaction textures in xenolithic high Mg–Al granulites at Anakapalle, eastern Ghats Belt, India: examples of contact polymetamorphism and infiltration-driven metasomatism. *Journal of Metamorphic Geology* **19**, 563–582.

Ritter, J. R. R. & Kaspar, T. (1997). A tomography study of the Chyulu Hills, Kenya. *Tectonophysics* **278**, 149–169.

Rudnick, R. L. (1992). Xenoliths—samples of the lower continental crust. In: Fountain, D. M., Arculus, R. & Kay, R. W. (eds) *Continental Lower Crust*. New York: Elsevier, pp. 269–316.

Rudnick, R. L., McDonough, W. F., McCulloch, M. T. & Taylor, S. R. (1986). Lower crustal xenoliths from Queensland, Australia: evidence for deep crustal assimilation and fractionation of continental basalts. *Geochimica et Cosmochimica Acta* **50**, 1099–1155.

Saggerson, E. P. (1963). *Geology of the Simba–Kibwezi area. Geological Survey of Kenya* **58**, 70 pp.

Sandiford, M. & Santosh, M. (1991). A granulite-facies kalsilite–leucite–hibonite association from Punalur, South India. *Mineralogy and Petrology* **43**, 225–236.

Sandiford, M., Neall, F. B. & Powell, R. (1987). Metamorphic evolution of aluminous granulites from Labwor Hills, Uganda. *Contributions to Mineralogy and Petrology* **95**, 217–225.

Santosh, M., Sandiford, M. & Reed, S. J. B. (1991). Zoned hibonite from Punalur, South India. *Mineral Magazine* **55**, 159–162.

Shackleton, R. M. (1973). Correlation of structures across Precambrian orogenic belts in Africa. In: Tarling, D. H. & Runcorn, S. K. (eds) *Implications of Continental Drift to the Earth Sciences*. London: Academic Press, pp. 1091–1095.

Shulters, J. C. & Bohlen, S. R. (1989). The stability of hercynite and hercynite–gahnite spinels in corundum- or quartz-bearing assemblages. *Journal of Petrology* **30**, 1017–1031.

Sills, J. D., Ackermand, D., Herd, R. K. & Windley, B. F. (1983). Bulk composition and mineral parageneses of sapphirine-bearing rocks along a gabbro–lherzolite contact at Finero, Ivrea Zone, Northern Italy. *Journal of Metamorphic Geology* **1**, 337–351.

Späth, A., Le Roex, A. P. & Opiyo-Akech, N. (2001). Plume–lithosphere interaction and the origin of continental rift-related alkaline volcanism—the Chyulu Hills Volcanic field, Southern Kenya. *Journal of Petrology* **42**, 765–787.

Stern, R. J. (1994). Arc assembly and continental collision in the Neoproterozoic East African orogen: implications for the conditions of Gondwanaland. *Annual Review of Earth and Planetary Sciences* **22**, 319–351.

Stern, R. J. & Dawoud, A. S. (1991). Late Precambrian (740 Ma) charnockite, enderbite, and granite from Jebel Moya, Sudan: a link between the Mozambique Belt and the Arabian–Nubian Shield? *Journal of Geology* **99**, 648–659.

Tenthorey, E. A., Ryan, J. C. & Snow, E. A. (1996). Petrogenesis of sapphirine-bearing metatroctolites from the Buck Creek ultramafic body, southern Appalachian. *Journal of Metamorphic Geology* **14**, 103–114.

Ulianov, A. G., Kalt, A. & Pettke, T. (2005). Hibonite, $Ca(Al,Cr,Ti,Si,Mg,Fe^{2+})_{12}O_{19}$, in granulite xenoliths from the Chyulu Hills volcanic field, Kenya. *European Journal of Mineralogy* **17**(2), 355–364.

Wells, P. R. A. (1977). Pyroxene thermometry in simple and complex systems. *Contributions to Mineralogy and Petrology* **62**, 129–139.

White, R. W. (1966). Ultramafic inclusions in basaltic rocks from Hawaii. *Contributions to Mineralogy and Petrology* **12**, 245–314.

Yakovlevskaya, T. A. (1961). Hibonite from Gornaya Shoriya. *Zapiski Vsesoyuznogo Mineralogicheskogo Obshchestva* **90**, 458–461 (in Russian).

Zandt, G., Gilbert, H., Owens, T. J., Ducea, M. & Saleeby, J. & Jones, C. H. (2004). Active foundering of a continental arc root beneath the southern Sierra Nevada in California. *Nature* **431**, 41–46.